

Multiple-Scattering Theory of X-Ray Magnetic Circular Dichroism: Implementation and Results for Iron K-edge

Ch. Brouder*

Laboratoire de Minéralogie-Cristallographie, CNRS URA9, Universités Paris 6 et 7, 4 place

Jussieu, 75252 Paris Cedex 05, France.

LURE, bât. 209D, F91405 Orsay Cedex, France.

M. Alouani

Department of Physics, The Ohio State University

Columbus Ohio 43210, USA.

K. H. Bennemann

Institut für Theoretische Physik, Arnimallee 14, D-14195 Berlin, Germany.

(August 8, 2018)

Abstract

An implementation of the multiple-scattering approach to x-ray magnetic circular dichroism (XMCD) in K-edge x-ray absorption spectroscopy is presented. The convergence problems due to the cluster size and the relativistic corrections are solved using an expansion of the Dirac Green function for complex energies up to the second order in $1/c$. The Fermi energy is dealt with via a complex plane integration. Numerical methods used to obtain the semi-relativistic Green function in the whole complex plane are explained. We present a calculation of the magnetic circular dichroism at the K-edge of bcc-iron including the core hole effect. A good agreement is found at high

energy. The physical origins of the XMCD spectrum near the edge and far from the edge are analyzed. The influence of the core hole, the possibility of a multiple-scattering expansion and the relation of XMCD with the spin-polarized density of states are discussed. A simple interpretation of XMCD at the K-edge is presented in terms of a rigid-band model.

78.70Dm, 78.20Ls, 75.10Lp, 75.50Bb

I. INTRODUCTION

X-ray magnetic circular dichroism (XMCD) in a magnetic sample is the difference between absorption spectra obtained from right- and left-circularly polarized x-rays. This experimental technique was discovered in 1987,¹ and gives information on the magnetic contribution of each orbital and of each atomic species in a sample. Still now, the detailed mechanisms that give rise to XMCD at the K-edge are not entirely clear near the edge and are unknown far from it. The purpose of the present paper is to understand XMCD at the K-edge over the whole energy range used in experiments. Our main tool is a new semi-relativistic equation which is very useful from a computational point of view, and which can be used to calculate other relativistic properties, such as magnetic anisotropy.

In a previous paper, we described a preliminary approach to the calculation of the x-ray magnetic circular dichroism effect in x-ray absorption spectroscopy, within the framework of the multiple-scattering theory.² We assumed that XMCD at the L_{II,III}-edges of rare earths and 5*d* transition metals has a simple interpretation and that XMCD at the K-edge was the most difficult case, because spin-orbit acts on the photoelectron, which makes a physical picture difficult to build. From the experience that was gained in the intervening years,³ we know now that the L_{II,III}-edges of rare earths are more complicated than expected, and some progress has been made towards a reliable practical use of the experimental results^{4,5} at the K-edge of transition metals.

Although fully relativistic calculations of XMCD at the K-edge are numerous,^{6–19} we believe that the use of a semi-relativistic approach is still justified. Its main advantage is that spin and space variables are uncoupled at the zeroth order. This enables us to use the full local cluster symmetry, to build a clearer physical picture, and to make orientation averages. The smaller scattering-matrix dimension of the semi-relativistic approach allows for the calculation of bigger clusters and broader energy ranges. Finally, the existing multiple-scattering numerical programs can be easily extended to calculate the XMCD. For instance, Ankudinov and Rehr have adapted their FEFF program²⁰ to calculate the extended structure

in XMCD at the $L_{II,III}$ -edge of rare earths and 5d transition metals. They obtained good agreement for gadolinium. A similar adaptation is possible, although more complex, for K-edge spectra.

Here we report on the calculation of the K-absorption spectra and the XMCD of Fe in the presence and absence of a static core hole in the $1s$ state. The influence of the core hole was taken into account by the final-state rule which assumes that the final state energies of the x-ray absorption process are measured in the presence of a static core hole, i.e., the dynamics of the excitation process are neglected.²¹ This rule has been used with success to explain the satellite structures on the high energy side of the emission spectra of simple metals.^{21,22} In particular, for Na and Al the $L_{II,III}$ emission satellites on the high-energy side of the main lines due to the double ionization of the $2p$ core level is well reproduced by the calculations if the excited atom is treated as an impurity and the static electron-hole interaction is included in the calculation.^{21,22} The final state rule was also used to calculate the L_{III} -edge of $3d$ transition metal ferromagnetics,²³ and the effect of the core hole is found to be very important. The determination of the self-consistent potentials is carried out within the local density approximation with a linear muffin-tin orbital (LMTO) basis-set.²⁴ We use a supercell geometry and treat the excited atom with a core hole as a single impurity atom in a lattice. A $1s$ electron is added to the conduction states in the supercell, and we let the system of $N+1$ electrons relax selfconsistently. We have found that the photo-electron localizes on the excited atom providing an efficient screening of the core hole. Like the case of $L_{II,III}$ edge²³ up to 80% of the photoelectron polarizes as a minority spin. Thus, the electronic structure of the excited Fe atom is very close to that of a cobalt metal. However, in this calculation we have found that the effect of the core hole on the K-absorption edge and the XMCD is small, and this is because the p -states of Fe are less affected by the presence of the core hole.

In this paper, the determination of the absorption spectra and the XMCD is carried out within the multiple scattering theory. During the implementation of our early formalism we encountered several difficulties that convinced us that the naive approach used in Ref. 2 to

take spin-orbit effect into account is mathematically not sound. In the present paper, we use a different mathematical framework for the calculation of XMCD, that can be generalized to take relativistic effects in the valence d -shell for $L_{II,III}$ -edges. This approach gives a direct expansion of the Dirac Green function in powers of $\frac{1}{c}$, it overcomes the divergence of the Foldy-Wouthuysen transformation through the use of complex energies, and it leads to results in reasonable agreement with experiment.

Some of our results are useful only for x-ray absorption spectroscopy, but others can have wider applications, such as the convergence of the semi-relativistic limit and the properties of the Green function at complex energies.

The remainder of the paper is organized as follows. In the second section we point out the limitation of the Foldy-Wouthuysen transformation and give a new method for the determination of the relativistic effects within the Green function approach. We then apply the Green function framework to the calculation of the XMCD signal. In a third section the use of complex energies is discussed, and a complex plane integration is used to take the Fermi energy into account. In the fourth section we present the numerical implementation that we used, and give the new XMCD cross-section formula at the K-edge. Finally, we present a calculation that was carried out on a reasonably large Fe cluster of 259 atoms near the edge and a cluster of 51 atoms up to 500 eV. Good agreement with experiment is found in the high-energy region. Various issues, such as the influence of the relativistic core hole, the origin of XMCD at the edge and far from it, the possibility of a multiple-scattering expansion are discussed. The spectra are related to the density of states through a simple rule, and the rigid-band model is found to be correct at high energy. An appendix showing how symmetrized bases were used to calculate XMCD faster and to understand some aspects of the experimental spectra closes the paper.

II. THE RELATIVISTIC EXPANSION

A. The Foldy-Wouthuysen transformation

The relativistic corrections to physical phenomena are usually treated using a perturbation approach developed in 1950 by Foldy and Wouthuysen (FW),²⁵ who made a unitary transformation to eliminate the coupling of the large small components from the Dirac equation and obtained, to zeroth order, the Pauli Hamiltonian and, to first order in $(1/c^2)$, the spin-orbit, Darwin and kinetic energy corrections. Later, this Hamiltonian was taken as a starting point for the calculation of many physical properties, such as magnetic anisotropy, XMCD or magneto-optic effects. Sometimes, the spin-orbit term is used in a second-order perturbation theory, overlooking that the FW-transformation must then also be made up to second order $(1/c^4)$ to achieve formal consistency. However, when carrying out higher-order transformations, strongly divergent terms are found even for the simple case of a hydrogen atom:²⁶ the second order “correction” is a sum of infinite terms. Additional information concerning the convergence properties of the FW-transformation can be found in Ref. 27.

Even at the $1/c^2$ order, the behavior of the Hamiltonian obtained by adding the kinetic energy correction to the non-relativistic Hamiltonian is so bad that all negative eigenvalues (bound states) disappear, and a continuum of states is obtained between $-\infty$ and $mc^2/4$, however small c may be.²⁸ In some cases,^{2,29} only the spin-orbit interaction is added to the non-relativistic Hamiltonian. For a Coulomb potential, the negative spin-orbit term pulls the particle into the singularity and the resulting Hamiltonian is not essentially self-adjoint (it can have any eigenvalue, depending on the chosen self-adjoint extension).^{30–32} Physically reasonable results could be obtained by choosing the boundary condition where the wave function is zero at $r = 0$ but this process is mathematically ambiguous.³²

To summarize, the series obtained from the FW-transformation exhibits three kinds of divergence: (i) the series itself diverges, which is usually not a problem since most perturbation series used in quantum mechanics are divergent (e.g. Zeeman effect, Stark effect, anharmonic oscillator);³³ (ii) from the second order term $(1/c^4)$, each term of the series is a sum of infinite terms that should add to a finite term, but no procedure is known to carry

out this summation;²⁶ (iii) the first order term of the series (spin-orbit coupling) diverges as the cluster size increases.

Recently, all these problems of the semi-relativistic limit were solved using modern mathematical methods, and we propose to use this new formulation for the calculation of XMCD. Other approaches to the semi-relativistic limit of the Dirac equation were proposed by quantum chemists.^{34,35}

B. Relativistic ($1/c$) expansion of the Green function

The standard method to calculate relativistic effects within the Green function approach is to consider the spin-orbit and other terms as a perturbation of the Hamiltonian, and to use the Lippmann-Schwinger equation corresponding to that perturbation.^{2,29} This procedure is not mathematically safe and leads to divergences. Another approach to XMCD was proposed by Natoli³⁶ where the Schrödinger equation including spin-orbit was solved for each muffin-tin sphere.

Here, we start from the retarded Green function $G^D(z)$ corresponding to the Dirac Hamiltonian with potential V (the Dirac Green function) and we use a slight modification of the analytic $1/c$ expansion of $G^D(z)$ that was obtained in Ref. 27 (see Ref. 37 for a detailed proof):

$$G^D(z) = [1 - T(z)]^{-1} \begin{pmatrix} G(z) & G(z)A^\dagger/(2mc) \\ AG(z)/(2mc) & [AG(z)A^\dagger + 2m]/(2mc)^2 \end{pmatrix} \quad (1)$$

where

$$T(z) = \begin{pmatrix} 0 & G(z)A^\dagger(V - z)/(2mc) \\ 0 & [AG(z)A^\dagger + 2m](V - z)/(2mc)^2 \end{pmatrix}. \quad (2)$$

All matrix entries are 2x2 matrices. $A = -i\hbar\sigma \cdot \nabla$ and σ are the Pauli matrices and $G(z)$ is the Green function for the Pauli Hamiltonian with potential V . V is generally a 2x2 matrix that describes the potential experienced by the electrons with up and down spins.

In the simplest case, V is a diagonal matrix made up of V^\uparrow and V^\downarrow . The successive terms of the relativistic expansion are obtained by the series $[1 - T(z)]^{-1} = 1 + T(z) + T^2(z) + \dots$. This expansion gives a very compact formulation of the correction terms. For instance, the first order correction to a non-degenerate bound-state eigenvalue E_0 corresponding to the eigenstate $|\psi\rangle$ is given by

$$\Delta E = \langle \psi | A^\dagger (V - E_0) A | \psi \rangle,$$

³⁸ which contains the kinetic energy correction, the Darwin correction and the spin-orbit correction. Because of this simplicity, formal manipulation can be carried out much further, for instance to obtain a consistent second order expansion of the spin-orbit interaction. Another aspect of this expansion is that the small components are not eliminated, which will be useful for x-ray absorption spectroscopy.

It was shown that expansion (1) is analytic,²⁷ but its actual radius of convergence was investigated only recently. Preliminary results^{39,40} for the Dirac Green function without potential showed that the radius of convergence was a function of the imaginary part of the energy. For a Dirac equation with potential, the Green function expansion could be shown⁴¹ to be convergent only when the imaginary part of the energy is greater than mc^2 (a very bad resolution indeed). However, the convergence can be much better when a physical property is calculated instead of the general Green function. For instance, the convergence of the bound state energy expansion is fast.^{39,42} Physically, the idea that can be drawn from these mathematical results is that the use of complex energies makes the semi-relativistic expansion converge, whereas it diverges on the real axis. This idea will be detailed in the next section.

From the formal point of view fully relativistic programs require a coupling of an infinity of different l values due to the magnetic field.⁴³ Up to now, the coupling between l and $l \pm 2$ was neglected, which limits the maximum possible value of l .⁴⁴ In our approach, this coupling is made consistently with $1/c$ through the expansion process.

C. Application to XMCD

In x-ray absorption spectroscopy, the spin-orbit parameter for the core hole has a magnitude of several hundreds of eV and cannot be considered *a priori* small. Furthermore, relativistic effects in x-ray absorption have been shown to be considerable both theoretically⁴⁵ and experimentally.⁴⁶ Therefore, a fully relativistic core hole wave function must be used. This is not possible within the standard semi-relativistic approach. In the electric dipole approximation, the relativistic formula for the x-ray absorption cross-section is:

$$\sigma(\hat{\epsilon}) = -4\pi\alpha_0\hbar\omega\langle i | (\hat{\epsilon}^* \cdot \mathbf{r}) \text{Im}[G^D(\mathbf{r}, \mathbf{r}'; z)] (\hat{\epsilon} \cdot \mathbf{r}') | i \rangle, \quad (3)$$

where $z = \hbar\omega + E_i + i\epsilon$, E_i is the energy of the core level $|i\rangle$ and $\hat{\epsilon}$ is the x-ray polarisation vector. The calculation of the fully relativistic initial state $|i\rangle$ presents no difficulty, thanks to the availability of Desclaux' program.⁴⁷ In Ref. 2 we supposed that the relativistic effects on the valence and continuum states are weak. We show in the present section that this supposition is not always true.

The influence of relativistic effects on the photoelectron is obtained by the series expansion of the Dirac Green function. The Dirac Green function in Eq.(1) is expanded up to second order in $1/c$:⁴⁸

$$\begin{aligned} \langle i | \hat{\epsilon}^* \cdot \mathbf{r} G^D \hat{\epsilon} \cdot \mathbf{r}' | i \rangle &\simeq \langle \phi | \hat{\epsilon}^* \cdot \mathbf{r} G \hat{\epsilon} \cdot \mathbf{r}' | \phi \rangle \\ &+ \frac{1}{2mc} \langle \phi | \hat{\epsilon}^* \cdot \mathbf{r} G A^\dagger \hat{\epsilon} \cdot \mathbf{r}' | \psi \rangle + \frac{1}{2mc} \langle \psi | \hat{\epsilon}^* \cdot \mathbf{r} A G \hat{\epsilon} \cdot \mathbf{r}' | \phi \rangle \\ &+ \frac{1}{(2mc)^2} \langle \phi | \hat{\epsilon}^* \cdot \mathbf{r} G A^\dagger (V - z) A G \hat{\epsilon} \cdot \mathbf{r}' | \phi \rangle \\ &+ \frac{1}{(2mc)^2} \langle \psi | \hat{\epsilon}^* \cdot \mathbf{r} (2m + A G A^\dagger) \hat{\epsilon} \cdot \mathbf{r}' | \psi \rangle \end{aligned} \quad (4)$$

where the two-component spinors $|\phi\rangle$ and $|\psi\rangle$ are the large and small components of the Dirac spinor $|i\rangle$. In our previous approach² we have neglected the relativistic nature of the core state, and used only the spin-orbit interaction, as a consequence we had obtained only the first and a part of the fourth term. Formula (4) is valid for a non-muffin-tin potential; the use of non-muffin-tin potentials is probably required to achieve a quantitative estimate

of XMCD. In all the terms of Eq. (4) only the fourth term yields magnetic circular dichroism for a powder sample. Therefore, in the following, we call σ_0 the spectrum obtained from the first term,

$$\sigma_0(\hat{\epsilon}) = -4\pi\alpha_0\hbar\omega \sum_s \langle \phi^s | (\hat{\epsilon}^* \cdot \mathbf{r}) \text{Im}[G(\mathbf{r}, \mathbf{r}'; z)] (\hat{\epsilon} \cdot \mathbf{r}') | \phi^s \rangle \quad (5)$$

where the sum over s is the sum over initial states (two spin states for a K-edge). For a powder, σ_0 does not depend on $\hat{\epsilon}$. We call σ_1 the spectrum obtained from the fourth term of Eq. (4).

$$\sigma_1(\hat{\epsilon}) = -4\pi\alpha_0\hbar\omega \sum_s \langle \phi^s | (\hat{\epsilon}^* \cdot \mathbf{r}) \text{Im} \left[G(z) \frac{A^\dagger(V-z)A}{(2mc)^2} G(z) \right] (\hat{\epsilon} \cdot \mathbf{r}') | \phi^s \rangle \quad (6)$$

and $\sigma_{MCD} = \sigma_1(\hat{\epsilon}^-) - \sigma_1(\hat{\epsilon}^+)$ for an external magnetic field aligned with the x-ray wavevector.

More precisely, we have in the fourth term:³⁸

$$A^\dagger(V-z)A = -\hbar^2 [(\nabla V \cdot \nabla) + (V-z)\Delta + i\sigma \cdot (\nabla V \times \nabla)]. \quad (7)$$

In the right-hand side of the above equation, only the third term contributes to XMCD at the K-edge, because the first two terms do not connect space and spin variables. In the case of spherical potentials, one obtains the usual formula for the spin-orbit interaction:⁴⁹

$$\xi(r) = -i \frac{\hbar^2}{(2mc)^2} \sigma \cdot (\nabla V \times \nabla) = \frac{\alpha_0^2 a_0^2}{4} \frac{1}{r} \frac{dV}{dr} \ell \cdot \sigma. \quad (8)$$

We took this formula for convenience, to make contact with Ref. 2, but it is also possible to act with A and A^\dagger directly on the Green function. This would be much simpler if all relativistic effects (and not only XMCD) were investigated.^{45,46} In principle, $\sigma_1(\hat{\epsilon}^-) + \sigma_1(\hat{\epsilon}^+)$ contributes also to the normal absorption spectrum, but this relativistic contribution was assumed to be small as compared to σ_0 .

Finally, to obtain the influence of all sites, the potential V must be written as a sum over all sites plus an interstitial potential. Because the operator A is translation invariant, each site can be taken as the origin when making transformation (8). In the muffin-tin case, it can be shown that the interstitial region does not contribute to XMCD.

For real energies, XMCD calculated within the present approach is formally identical with the results of Ref. 2. Therefore, we can use the latter to understand the real energy behavior of the former. For small clusters, the calculation of XMCD was easy,⁵⁰ but as the cluster size increased, we met difficulties. Fig. 1 shows σ_0 and σ_{MCD} for a cluster of 259 atoms of bcc-Fe. Both spectra exhibit a very sharp resonance (width ≈ 0.005 eV). This resonance is due to the fact that, as the cluster size increases, one comes close to the singularities of the crystal scattering matrix.⁵¹ The second point is that σ_{MCD} is larger than σ_0 . This unphysical result proves that the spin-orbit effect is not a small perturbation of the system in that energy range. This illustrates the fact, discussed in the previous section, that the relativistic expansion is generally not convergent at real energies. It may be worthwhile noticing that this divergence of the relativistic expansion is not due to the Z/r^3 singularity of the spin-orbit interaction in a Coulomb potential.

Moreover, the experimental resolution at the K-edge of transition metals is of the order of 1 eV whereas Fig. 1 shows much sharper structure. Therefore, the usual method of convoluting the theoretical spectrum with a Lorentzian profile for comparison with experiment would mean calculating much more points than actually needed.

For real potentials, the singularities of the multiple-scattering matrix are on the real axis, and the use of a complex energy smoothes the sharp structure of σ_0 linked with the cluster size. We show in the next section that the convergence problem of the relativistic expansion is also solved by calculating the Green function at complex energies.

Finally, we work within a real space multiple-scattering approach, so that the cluster is assumed to be of finite size. The relativistic expansion of the Green function for an infinite crystal was studied in Ref. 52.

III. COMPLEX ENERGIES

In this section, we justify the use of complex energies, and we show how this simplifies the calculation of physical quantities. We assume that the potential V is a diagonal 2x2

matrix made up of V^\uparrow and V^\downarrow , which are the potentials experienced by up and down spins. These potentials are assumed to be real. The generalization to complex potentials is a non-trivial task,⁵³ and the use of an energy-dependent width $\Gamma(E)$, which can be considered to be the imaginary part of the potential (constant over space), was found to be sufficient to reproduce experimental spectra.⁵⁴

A. Green function

The link between the wave function and the Green function formulae for x-ray absorption cross-section is established through the identity:⁵⁵

$$\sum_f |f\rangle\langle f| \delta(E - E_f) = \delta(E - H) = -\frac{1}{2\pi i} [G^+(E) - G^-(E)], \quad (9)$$

where $G^\pm(E) = G(E \pm i\epsilon)$, ϵ is a positive number that is taken to tend to zero at the end of the calculation (this is just a notation to designate an integration path in the complex plane).

Because of the finite core-hole lifetime, the calculated spectrum must be convoluted by a Lorentzian with a half width at half maximum (HWHM) Γ (which may ultimately depend on the photoelectron energy). In the Green function formalism, the convolution with a Lorentzian is obtained by calculating the Green function for a complex energy.⁵⁶ This can be shown from the formula:

$$\int_{-\infty}^{+\infty} de \frac{\Gamma G^+(e) - G^-(e)}{\pi (E - e)^2 + \Gamma^2} = G(E + i\Gamma) - G(E - i\Gamma). \quad (10)$$

Since $G(\mathbf{r}, \mathbf{r}'; z) = G(\mathbf{r}', \mathbf{r}; z)$ ⁵³ and $G(\mathbf{r}, \mathbf{r}'; z)^* = G(\mathbf{r}', \mathbf{r}; z^*)$ for Hermitian potentials V , we have $G(E - i\Gamma) = G(E + i\Gamma)^*$.

Moreover, the term $\hbar\omega = e - E_i$ of the absorption cross-section can be taken care of by noticing that $zG(z) = HG(z) + 1$. Thus $eG^\pm(e) = HG^\pm(e) + 1$, which gives, after convolution, $HG(E + i\Gamma) + 1 = (E + i\Gamma)G(E + i\Gamma)$.

Therefore

$$\sigma_0(\hat{\epsilon}) = -4\pi\alpha_0 \langle i | (\hat{\epsilon}^* \cdot \mathbf{r}) \text{Im}[(E + i\Gamma - E_i)G(\mathbf{r}, \mathbf{r}'; E + i\Gamma)](\hat{\epsilon} \cdot \mathbf{r}') | i \rangle. \quad (11)$$

In other words, the convoluted spectrum is obtained by calculating the Green function for an energy with an imaginary part Γ .

B. Fermi energy

In the previous section, we did not take into account that all one-electron states up to the Fermi energy E_F are occupied. To yield physical results, integral (10) must be carried out from E_F instead of from $-\infty$. This modifies our expression in an interesting way. We must now evaluate :

$$\begin{aligned} & \frac{1}{2i} \int_{E_F}^{+\infty} de \frac{\Gamma (e - E_i)(G^+(e) - G^-(e))}{\pi (E - e)^2 + \Gamma^2} = \\ & \frac{1}{4\pi} \int_{E_F}^{+\infty} de (e - E_i)(G^+(e) - G^-(e)) \left[\frac{1}{E - e + i\Gamma} - \frac{1}{E - e - i\Gamma} \right]. \end{aligned} \quad (12)$$

This integral can be calculated by a complex plane integration technique:⁵⁷ Since the self-consistent potential V is Hermitian, the poles of $G^+(e)$ are at $e = r - i\epsilon$, where r is a real number. Therefore, we can choose the contour of Fig. 2 to apply Cauchy's integral formula.⁵⁸ The contribution of the Jordan contour at infinity is zero⁵⁹ and we obtain:

$$\begin{aligned} & \frac{1}{2i} \int_{E_F}^{+\infty} de \frac{\Gamma (e - E_i)G^+(e)}{\pi (E - e)^2 + \Gamma^2} = -\frac{i}{2}\theta(E - E_F)(E + i\Gamma - E_i)G(E + i\Gamma) \\ & + \frac{\Gamma}{\pi} \int_0^\infty dt \frac{(E_F + it - E_i)G(E_F + it)}{(E_F + it - E)^2 + \Gamma^2}. \end{aligned} \quad (13)$$

Heavyside's step function $\theta(E - E_F)$ is present in the expression because, when $E > E_F$, the pole $E + i\Gamma$ is inside the contour.

The second integral in the rhs of Eq. (12) is closed on the negative imaginary side, and we obtain finally:

$$\begin{aligned} & \int_{E_F}^{+\infty} de \frac{\Gamma (e - E_i)\text{Im}[G^+(e)]}{\pi (E - e)^2 + \Gamma^2} = \theta(E - E_F)\text{Im}[(E + i\Gamma - E_i)G(E + i\Gamma)] \\ & + \frac{\Gamma}{\pi} \int_0^\infty dt \text{Re} \left[\frac{(E_F + it - E_i)G(E_F + it)}{(E_F + it - E)^2 + \Gamma^2} \right]. \end{aligned} \quad (14)$$

It can be shown that the right-hand side of Eq. (14) is continuous at $E = E_F$ in spite of the step function.⁶⁰ The recourse to this contour integration is efficient, as compared to an integration over real energies, because the Green function is quite smooth on the line $z = E_F + it$ (see Fig. 3) and only a few points must be calculated to evaluate the integral. Moreover, $G(E_F + it)$ tends rapidly to the local atomic Green function of the absorbing site, as shown in Fig. 3. Therefore, $G(E_F + it)$ can be obtained at high t just by calculating a simple one-site Green function. The vanishing of the neighbor's influence can be understood through the form of the structure constant matrix H (see section IV). The H -matrix elements have the form $H^{ij} = \exp(i\kappa R_{ij})P(1/\kappa R_{ij})$ where P is a polynomial. For large t , $\kappa = \sqrt{z} \simeq \sqrt{t/2}(1 + i)$, and the H -matrix elements describing the influence of the neighbors are damped by a factor of $\exp(-\sqrt{t/2}R_{ij})$. The integration in the complex plane was chosen along a straight line. This is not a steepest descent path but was found to be sufficiently efficient.

The above proofs are the same whether $G(z)$ is the non-relativistic or the relativistic Green function (assuming that the negative energy states are full). To obtain the expression for σ_1 after convolution, we start from the results obtained with the Dirac Green function and use the relativistic expansion (4). This gives an expression for σ_1 which is the sum of Eq. (6) for $z = E + i\Gamma$ and of an integral over the line $z = E_F + it$. The detailed form of the result will be given in section IV C.

It was observed by Rehr⁶¹ that thermal motion can also be a convergence factor in multiple-scattering calculations. Although thermal effects can be formally accounted for in full multiple-scattering calculations,⁶² temperature effects were neglected in the present study.

Finally, a characteristic of the $1/c^2$ relativistic term is that spin-flip is not allowed for powders. An explicit calculation of the spin-flip scattering amplitude shows that it is an order of magnitude smaller than non-spin-flip scattering for Nd^{3+} .⁶³ Experiments⁶⁴ confirm that elastically scattered electrons are rarely spin-flipped.

IV. NUMERICAL ASPECTS

The x-ray absorption cross-section is obtained from the cluster Green function for complex energies, which we write as^{65,37}

$$G(\mathbf{r}_i, \mathbf{r}'_j; z) = -i\kappa t_\ell^i \sum_{\ell m} \frac{R_\ell^i(r_<) Y_\ell^m(\hat{r}_i)}{\sin \delta_\ell^i} H_\ell^i(r_>) Y_\ell^{m*}(\hat{r}'_j) \delta_{i,j} + \kappa^2 \sum_{\ell m \ell' m'} \frac{R_\ell^i(r_i) Y_\ell^m(\hat{r}_i)}{\sin \delta_\ell^i} \left(\tau_{\ell m \ell' m'}^{ij} + \frac{t_\ell^i}{\kappa} \delta_{\ell, \ell'} \delta_{m, m'} \delta_{i,j} \right) \frac{R_{\ell'}^j(r'_j) Y_{\ell'}^{m'*}(\hat{r}'_j)}{\sin \delta_{\ell'}^j} \quad (15)$$

where $\kappa = \sqrt{z}$, δ_ℓ^i is the (complex) phase-shift for potential $V^i(r)$, $t_\ell^i = \sin \delta_\ell^i \exp i\delta_\ell^i$, $R_\ell^i(r)$ is the regular solution of the radial Schrödinger equation for potential $V^i(r)$ that matches smoothly to $\cos \delta_\ell^i j_\ell(\kappa r) - \sin \delta_\ell^i n_\ell(\kappa r)$ at the muffin-tin radius ρ_i , $H_\ell^i(r)$ is the irregular solution of the radial Schrödinger equation for potential $V^i(r)$ that matches smoothly to $h_\ell^+(\kappa r)$ at the muffin-tin radius. Finally the multiple-scattering matrix is $\tau = [T_a^{-1} - \kappa H]^{-1}$, where $(T_a)_{\ell m \ell' m'}^{ij} = -(t_\ell^i/\kappa) \delta_{i,j} \delta_{\ell, \ell'} \delta_{m, m'}$ and $H_{\ell m \ell' m'}^{ij} = -4\pi i \sum_{\lambda \mu} i^{\ell+\lambda-\ell'} C_{\ell m \lambda \mu}^{\ell' m'} h_\lambda^+(\kappa R_{ij}) Y_\lambda^\mu(\hat{R}_{ij})$. In the last expression, the Hankel function h_λ^+ is defined as the function $h_\lambda^{(1)}$ of Ref. 66. This straightforward extension of the real energy case is possible because wave functions and phase-shifts are analytical functions of κ .⁶⁷

We present here the numerical methods that were used to calculate the Green function and the ground state. First, we describe how the radial wave functions were obtained, then we show how the Green function singularities were avoided, and finally we explain how the multiple-scattering matrix was calculated.

A. Radial wave functions

The core level energy and wavefunction were obtained from the Dirac SCF program of Desclaux.⁴⁷

The photoelectron wave functions were obtained by adapting the method of Ref. 68 to complex energies. A non-normalized regular wave function is written as $\underline{R}_\ell(r) = r^\ell f_\ell(r)$ with $f_\ell(r) = f_r(r) + i f_i(r)$. For the complex energy $E = E_r + i E_i$ the radial Schrödinger equation is :

$$\begin{aligned}
f_r'' &= (V(r) - E_r)f_r - \frac{2(\ell + 1)}{r}f_r' + E_i f_i \\
f_i'' &= (V(r) - E_r)f_i - \frac{2(\ell + 1)}{r}f_i' - E_i f_r,
\end{aligned} \tag{16}$$

with the boundary conditions $f_r(0) = 1$, $f_r'(0) = -Z/(l + 1)$, $f_i(0) = 0$, $f_i'(0) = 0$. Where f' and f'' are, respectively, the first and second radial derivatives of f . This system of second order differential equations is transformed into a system of four first order differential equations which is solved by a forward step-adaptative fourth-order Runge-Kutta method.⁶⁹

The phaseshifts δ_ℓ are deduced from the Wronskian equation :

$$\exp(2i\delta_\ell) = -\frac{h_\ell^-(\kappa\rho)\underline{R}_\ell'(\rho) - \kappa h_\ell^{-'}(\kappa\rho)\underline{R}_\ell(\rho)}{h_\ell^+(\kappa\rho)\underline{R}_\ell'(\rho) - \kappa h_\ell^{+'}(\kappa\rho)\underline{R}_\ell(\rho)}. \tag{17}$$

The normalized radial wave functions $R_\ell^i(r)$ are obtained from $\underline{R}_\ell^i(r)$ and the phaseshifts.

The irregular wave function is written as $H_\ell = r^{-(\ell+1)}g_\ell(r)$ with $g_\ell(r) = g_r(r) + ig_i(r)$ and obtained by backward step-adaptative fourth-order Runge-Kutta method⁶⁹ from the boundary conditions $H_\ell(\rho) = h_\ell^+(\kappa\rho)$, $H_\ell'(\rho) = \kappa h_\ell^{+'}(\kappa\rho)$.

B. Multiple-scattering matrix and singularities in the Green function

Formula (62) of Ref. 2 could not be directly applied because of possible infinite normalization factors arising from the matching of the wave function at the muffin-tin radius to a sum of Bessel functions.⁷⁰ With the present normalization at the muffin-tin radius, the radial wave functions cannot be singular, but $\sin\delta_\ell^i$ terms arise in the denominator of the Green function (see Eq. 15). Therefore, we must examine the behavior of the scattering matrix when $\sin\delta_\ell^i$ becomes small.⁵⁰ We have

$$\tau = T_a[1 - \kappa HT_a]^{-1} = T_a + \kappa T_a[1 - \kappa HT_a]^{-1}HT_a. \tag{18}$$

Hence,

$$\tau_{\ell m \ell' m'}^{ij} = -\frac{1}{\kappa} \sin\delta_\ell^i e^{i\delta_\ell^i} \left[\delta_{i,j} \delta_{\ell,\ell'} \delta_{mm'} + \left([1 - \kappa HT_a]^{-1} H \right)_{\ell m \ell' m'}^{ij} \sin\delta_{\ell'}^j e^{i\delta_{\ell'}^j} \right], \tag{19}$$

and we see that $\tau_{\ell m \ell m}^{ii} / \sin^2 \delta_\ell^i$ is generally singular at $\sin \delta_\ell^i = 0$ because of the first term. These singularities did not appear in previous calculations of x-ray absorption cross section because $\text{Im}(\tau)$ was used, which is regular since an additional $\sin \delta_\ell^i$ factor comes from $e^{i\delta_\ell^i}$. To avoid these singularities, one can use $(\tau_{\ell m \ell m}^{ii} + t_\ell^i / \kappa) / \sin^2 \delta_\ell^i$, which is smooth. Therefore, all terms of the Green function (15) are regular.

To avoid the singularities discussed in the previous section, and to use a more symmetric equation, we use a polar decomposition technique⁷¹ and define a modified multiple scattering matrix $\tilde{\tau}$ by $\tau = T_a + \sqrt{T_a} \tilde{\tau} \sqrt{T_a}$. Numerically, $\tilde{\tau}$ is obtained from the equation :

$$\tilde{\tau} = [1 - \kappa \sqrt{T_a} H \sqrt{T_a}]^{-1} - 1. \quad (20)$$

$\tilde{\tau}$ is a regularized multiple-scattering matrix that describes the effect, on each atom, of the rest of the cluster ($\tilde{\tau}$ is zero for a cluster of one atom). The matrix elements of $[1 - \kappa \sqrt{T_a} H \sqrt{T_a}]$ are calculated from the phaseshifts and from the efficient algorithm for the calculation of H that was proposed by Rehr and Albers⁷² and tested against alternative methods.⁷³ The form $[1 - \kappa \sqrt{T_a} H \sqrt{T_a}]^{-1}$ combines the advantages of the two standard equations $\tau = [T_a^{-1} - \kappa H]^{-1}$ and $\tau = T_a [1 - \kappa H T_a]^{-1}$. As in the first equation, a symmetric matrix is inverted (when real spherical harmonics are used), so that fast inversion algorithms for symmetric matrices can be used.⁷⁴ As in the second equation, it is regular when $(T_a)_{\ell m \ell' m'}^{ij} = 0$, so that spurious singularities of T_a^{-1} are very simply avoided.⁷⁵ Moreover, asymptotic analysis⁶² shows that it is well behaved when ℓ is large and/or κ is small, whereas none of the two standard equations is. The matrix is inverted using a standard LU decomposition technique.⁶⁹

C. Cross-sections

The detailed expression of the absorption and XMCD cross-sections for a powder relies on the orientational averaging technique used in Ref. 2, and more calculation steps are given in Ref. 50. As in Eq. (14), all cross sections are written as the sum of a Green function term

and an integral. With our modified multiple-scattering matrix, the ‘‘Green function’’ part of the K-edge absorption cross sections at energy $E = \hbar\omega + E_i$ with a HWHM Γ becomes:

$$\sigma_0 = \sum_s \text{Im} [\tilde{\sigma}_{0a}^s(E + i\Gamma) + \tilde{\sigma}_{0n}^s(E + i\Gamma)] \quad (21)$$

where the sum over s is the sum over the two spin states (i.e. the sum of the cross-sections calculated for potentials V^\uparrow and V^\downarrow). For each spin state one defines $\tilde{\sigma}_{0a}(z) = (4\pi\alpha_0/3)(z - E_i)i\sqrt{z} \exp[i\delta_1^0(z)]D^H(z)$, which is the atomic contribution to x-ray absorption, and

$$\tilde{\sigma}_{0n}(z) = (4\pi\alpha_0/3)(z - E_i)\sqrt{z}D^2(z) \exp[i\delta_1^0(z)] \frac{\tilde{\tau}^{00}(11, 00; z)}{\sqrt{3} \sin \delta_1^0(z)} \quad (22)$$

which describes the influence of the neighbors ($i = 0$ denotes the absorbing site). We recall that² $\tilde{\tau}^{0j}(1\ell, a\alpha; z) = \sum_{\mu m} (-1)^{(1-\mu)} (1 - \mu\ell m | a\alpha) \tilde{\tau}_{1\mu\ell m}^{0j}(z)$.

The radial integrals are $D(z) = \int_0^\infty r^3 dr \phi_0(r) R_1^0(r; z)$, where $\phi_0(r)$ is the large component of the core hole wave function and $D^H(z) = \int_0^\infty r^3 dr \phi_0(r) F(r; z)$ where $F(r, z)$ is an auxiliary function defined as $F(r; z) = \int_0^\infty r'^3 dr' \phi_0(r') R_1^0(r_<; z) H_1^0(r_>; z)$ (R_ℓ^i and H_ℓ^i are defined in section IV A).

The ‘‘Green function’’ part of the magnetic circular dichroism cross-section is written:

$$\sigma_{MCD} = \text{Im} \left[\sum_s ((-1)^{(s-1/2)} (\tilde{\sigma}_{1a}^s(E + i\Gamma) + \tilde{\sigma}_{1l}^s(E + i\Gamma) + \tilde{\sigma}_{1n}^s(E + i\Gamma))) \right] \quad (23)$$

where $\tilde{\sigma}_{1a}(z) = (4\pi\alpha_0/3)(z - E_i)z \exp[2i\delta_1^0(z)]M^{HH}(z)$ describes the purely atomic contribution to XMCD (the Fano effect),

$$\tilde{\sigma}_{1l}(z) = -(4\pi\alpha_0/3)(z - E_i)2iz \exp[2i\delta_1^0(z)]D(z)M^H(z) \frac{\tilde{\tau}^{00}(11, 00; z)}{\sqrt{3} \sin \delta_1^0(z)} \quad (24)$$

is the local contribution due to the spin-polarization of the p -states on the absorbing site, and

$$\begin{aligned} \tilde{\sigma}_{1n}(z) &= (4\pi\alpha_0/3)(z - E_i)zD^2(z) \sum_{j\ell} \frac{(-1)^\ell}{12} \exp[i(\delta_1^0(z) + \delta_\ell^j(z))] \zeta_\ell^j(z) \\ &\times \sum_{a=|\ell-1}^{\ell+1} [(\ell - a)(\ell + a + 1) + 2] \sum_\alpha (-1)^{a-\alpha} \frac{\tilde{\tau}^{0j}(1\ell, a\alpha; z)\tilde{\tau}^{0j}(1\ell, a-\alpha; z)}{\sin \delta_1^0(z) \sin \delta_\ell^j(z)} \end{aligned} \quad (25)$$

describes the contribution to XMCD due to the spin-orbit scattering of the photoelectron by the neighbors and the absorber. The radial matrix elements are $M^H(z) = \int_0^\infty r^2 dr \xi(r) R_1^0(r; z) F(r; z)$, $M^{HH}(z) = \int_0^\infty r^2 dr \xi(r) F^2(r; z)$ and $\zeta_\ell^j(z) = \int_0^\infty r^2 dr \xi^j(r) [R_\ell^j(r; z)]^2$, with $\xi(r)$ as defined in Eq. (8).

The analysis of §IV B shows that $\tilde{\tau}^{0j}(1\ell, a\alpha; z)$ can be divided by $\sqrt{\sin \delta_1^0(z) \sin \delta_\ell^j(z)}$, and all terms of the XMCD cross-section are now regular.

For each term, the presence of the Fermi energy is taken into account by calculating integrals along the line $e = E_F + it$ as in Eq. (14): to all $\text{Im}[\sigma(E + i\Gamma)]$ terms we add the integral:

$$\frac{\Gamma}{\pi} \int_0^\infty dt \text{Re} \left[\frac{\sigma(E_F + it)}{(E_F + it - E)^2 + \Gamma^2} \right]. \quad (26)$$

V. RESULTS

The converged potentials used in the multiple scattering formalism were obtained by means of an all-electron self-consistent, scalar-relativistic and spin-polarized linear-muffin-tin orbital (LMTO) method.²⁴ We used the exchange-correlation potential and energy in the von Barth and Hedin approximation.⁷⁶ For the Brillouin zone integration of the density of states we used the tetrahedron method with about 300 \mathbf{k} points in the irreducible part of the Brillouin zone.⁷⁷ To simulate the effect of the core hole, we treated the excited atom as a single impurity in a lattice using a supercell geometry. We have used increasingly larger supercells to ensure the convergence of the magnetic moment and the density of states of the impurity site. The final calculations were done for a simple cubic lattice of 16 atoms per unit cell; the lattice parameter being $a = 2a_0$. The results for the magnetic moment and the density of states are close to those of the supercell of 4 atoms. To use larger clusters in the multiple-scattering formalism we had to assume that the potentials for distant shells are bulk like.

A. Near edge region

Fig. 4 a and b show the results we obtained for a converged cluster of 259 atoms of bcc-iron (diameter 2.0 nm). The convergence was investigated by checking that the spectral shape becomes stable with respect to the cluster diameter and by comparing to the results obtained with a cluster of 821 atoms (diameter 2.9 nm) on a wider energy mesh. The potentials for the initial state (without core hole) and for the final state (with core hole) were obtained by a self-consistent super-cell calculation as indicated above. We used touching muffin-tin spheres without overlap. Because of the core hole width ($\Gamma = 2$ eV), absorption is possible at energies lower than the Fermi level. The effect of the Fermi level is clear, especially for the XMCD spectrum. With a Fermi level $E_F = 2$ eV, the first positive structure disappears whereas with $E_F = -2$ eV, it is too large. Therefore, the size of the first positive peak depends strongly on the position of the Fermi level.

The absorption and XMCD cross-sections are now smooth and the divergences due to the cluster size and the relativistic corrections have disappeared. We see also that the spectra are continuous at the Fermi energy, although they are given by two different formulas for $E > E_F$ and $E < E_F$. This corroborates the fact that our treatment of the Fermi level is numerically sound.

Figure 5 compares our calculation with experiment for the edge region. All experimental and theoretical spectra were normalized so that the absorption edge jump is 1. The normal spectrum is not well reproduced. The agreement for the XMCD spectrum is better, although the excellent agreement in the intensity of the first two peaks is fortuitous, because the degree of circular polarization was not one for the experimental spectrum. For the calculated spectrum, various contributions are presented. The full thick line is the total contribution, and the full thin line is the local contribution ($\tilde{\sigma}_{1l}$ of Eq. (24)). In Fig. 6, $\tilde{\sigma}_{1n}$ as written in Eq.(25) is expanded into the contribution of each ℓ ($\ell=1,2,3$) and $j=0,1,2$ (absorbing atom, first shell, second shell). For later use, the results are given without taking Fermi energy into account. No term $\ell=0$ exists because $\ell=0$ gives no spin-orbit. For the absorbing site,

the terms with even ℓ are zero because of symmetry. From Fig. 6, it can be observed that the first positive peak (peaking at 1 eV) is not due to the local term (24), but to the spin-polarization of the d -states of the neighbors (mainly the term corresponding to $\ell=2$ and $j=1$ in Eq. (25)). This is related to the weak ferromagnetic nature of bcc-Fe,⁴ and was already observed on a smaller cluster⁵⁰ and in tight-binding calculations.^{78,79} Both absorption and XMCD calculated structures are too large from 20 eV above the edge. This reduction, which is very common in multiple-scattering calculations, is probably due to photoelectrons that experience inelastic interaction with the metal. This inelastic effect comes into play above the plasmon energy (about 10 eV) and can be included in our calculation through an energy-dependent Γ .^{54,80} The main failure of the XMCD calculation is the presence of a large second positive peak which is absent in the experiment. A similar peak can be observed in fully-relativistic⁶ and tight-binding calculations,^{78,79} although a direct comparison is difficult because of the different normalization used.

B. Core hole

Two modifications of the core hole were tested. In the first one, the non relativistic (Schrödinger) equation was solved for the core hole. The core hole energy was found different, but the $1s$ wavefunction was quite similar to the relativistic one, and the normal spectrum was a bit smaller (because the normalization of the relativistic wavefunction includes the small component, which does not contribute to the spectrum) but the XMCD spectrum was not distinguishable from the relativistic result. Similarly, core hole exchange splitting is negligible since the difference between the core states obtained with up and down potentials did not yield noticeable effects.

The second test was conducted to test the influence of the core hole on the spectra. Fig. 7 shows the normal and XMCD spectra with and without core hole and with a Fermi energy $E_F=0$ eV). The normal spectra are quite similar, except for an overall amplitude factor. The XMCD spectra are more different, although the position of the structure does

not move. Comparison with experiment does not enable us to decide for a model.

C. SPEXAFS

In XMCD at the K-edge, spin-orbit acts directly on the photoelectron, and it is interesting to know whether the high-energy part of the spectrum is related to the spin polarization of the p -states of the absorbing site. Using the methods developed in Ref. 81, it is possible to show that, in the single scattering approximation, only the p -projected term $\tilde{\sigma}_{1l}^{\uparrow} - \tilde{\sigma}_{1l}^{\downarrow}$ survives at high energy. Figure 8(b) shows the spectrum obtained with a cluster of 51 atoms, calculating all angular momenta up to $\ell=8$, and multiplied by 1/3. The cluster is too small to be realistic in the edge region, but above 30 eV, the overall agreement is correct. The peak at 110 eV in the theoretical spectrum should be broadened, and the peak at 60 eV in the experimental spectrum is probably due to multielectronic effects, which are known to be strong in XMCD spectra at that energy.⁸² The thin line represents the contribution of the p -projected states, which is seen to be dominant at high energy. Moreover, the calculated XMCD spectrum is in phase with the calculated EXAFS spectrum. This phase relation between dichroic and normal spectra was observed experimentally by Pizzini and coll.⁴

It is sometimes assumed that XMCD reflects the spin-polarization of p states projected on the absorbing atom ($\rho^{\uparrow} - \rho^{\downarrow}$). Fig. 9 shows that the absorption spectrum is indeed quite similar to the p density of states, but the XMCD spectrum is quite different from the spin polarization of the p density of states. In fact, the spin-polarization is very similar to the derivative of the density of states. In other words, the rigid band model becomes correct at high energy (a somewhat surprising result), and the band splitting is about 1 eV.

From this result, a very simple approximate expression can be derived for XMCD. Assuming a rigid band model, we can consider that the up and down bands are exchange-split by the energy ΔE . Moreover, neglecting the non-diagonal terms of the spin-orbit operator, one can consider that the $m = \pm 1$ components of the p -band are split by spin-orbit coupling $\zeta l.s$. Therefore, for transitions towards $\ell = 1, m = 1$ final states (left-circularly

polarized x-rays), we have

$$\sigma^{+\uparrow} = \sigma(E + \Delta E/2 - \zeta) \quad (27)$$

$$\sigma^{+\downarrow} = \sigma(E - \Delta E/2 + \zeta) \quad (28)$$

$$\sigma^+ \simeq 2\sigma(E) + (\Delta E/2 - \zeta)^2 d^2\sigma/dE^2 \quad (29)$$

and for transitions towards $\ell = 1, m = -1$ final states (right-circularly polarized x-rays):

$$\sigma^{-\uparrow} = \sigma(E + \Delta E/2 + \zeta) \quad (30)$$

$$\sigma^{-\downarrow} = \sigma(E - \Delta E/2 - \zeta) \quad (31)$$

$$\sigma^- \simeq 2\sigma(E) + (\Delta E/2 + \zeta)^2 d^2\sigma/dE^2 \quad (32)$$

therefore, XMCD becomes

$$\sigma^+ - \sigma^- \simeq -2\Delta E\zeta d^2\sigma/dE^2. \quad (33)$$

Since ζ is fairly constant at high energy, the exchange-splitting energy ΔE can be deduced from experimental spectra. Figure 10 shows XMCD together with the second derivative of the normal spectrum (multiplied by 10). Because the model is very crude, the agreement is not perfect, but good enough to say that the image deduced from the rigid-band model is correct. The presence of this second derivative explains also the phase relation between EXAFS and XMCD (considering EXAFS as a sum of sines). A more elaborate interpretation comes from considering the expression for $\tilde{\sigma}_{0n}$ (Eq. (22)) and $\tilde{\sigma}_{1l}$ (Eq. (24)). Both expressions involve the multiple-scattering matrix $\tilde{\tau}^{00}(11, 00; z)$, but $\tilde{\sigma}_{1l}$ contains an additional factor i that makes it proportional to the real part of $\tilde{\tau}^{00}(11, 00; z)$, whereas the EXAFS cross section is proportional to its imaginary part (it was checked that the other factors do not intervene much in the phase at high energy). Since real and imaginary part of the Green function are related by Kramers-Kronig theorem, which transforms sine functions into cosine functions, and because dichroic effect is due to the difference between spin up and spin down $\tilde{\sigma}_{1l}$, it is proportional to the derivative of the real part of $\tilde{\tau}^{00}(11, 00; z)$ which, because of an additional minus sign, is in phase with the imaginary part of the multiple-scattering matrix

(to see this, consider that, in the EXAFS regime, the Green function can be approximate by $\exp(ikR + \phi)$, the imaginary part is a sine function - the EXAFS formula - and the derivative of the real part is a sine function as well). Of course, this correspondence between XMCD and EXAFS is not exact, and much interesting information comes from the difference.

D. Multiple-scattering expansion

The program that we used to calculate the XMCD spectrum of iron is relatively heavy and slow. To make the analysis of XMCD spectra as easy as that of normal absorption spectra, it is necessary to investigate the validity of the multiple-scattering expansion which is used by much faster programs, such as FEFF.⁶¹ To do this, we compare the results obtained by the full inversion of $(1 - \kappa T_a H)^{-1} T_a$ with the single scattering expansion $(T_a + \kappa T_a H T_a + \kappa^2 T_a H T_a H T_a)$ and the double-scattering expansion (previous term plus $\kappa^3 (T_a H)^3 T_a$). This comparison is shown in Fig. 11. The overall agreement is correct but not excellent, probably because of the shadowing effect which is large in bcc structures. Notice that, in principle, the zeroth-order scattering $(T_a + \kappa T_a H T_a)$ also contributes due to the term $\tilde{\sigma}_{1n}$. However, this contribution is very small at high energy. Higher order terms are considered in Ref. 83.

VI. CONCLUSION

Since the first experimental XMCD spectra,¹ a number of calculations of XMCD K-edge spectra have been carried out, using different methods. A fully relativistic KKR method was used for bcc-Fe,^{6-9,11,12} hcp-Co,^{9,13} Fe-Co alloys,^{10,14-16,18,19} and fcc-Ni.¹¹ A relativistic LMTO-ASA calculation of the K-edge XMCD spectrum of Fe in GdFe₂ was carried out in Ref. 17, a molecular orbital approach was used for Fe in tetrahedral and octahedral environments,⁸⁴ a multiplet approach for Ni in a molecular magnet⁸⁵ and a tight-binding method for metallic Fe and Ni^{78,79} and Co,⁷⁹ where XMCD was related to the projection of the orbital momentum along the x-ray direction. All these calculations were restricted to a narrow energy range around the edge. We have developed in this paper a multiple-scattering

approach which allows for the calculation of extended structure, and includes the core hole without additional effort.

We have presented a solution of the convergence difficulties associated to the one-electron calculation of physical properties related to spin-orbit interaction. A recourse to Green functions with complex energy argument led us to smooth absorption and XMCD cross-sections. The presence of the Fermi level was accounted for through a complex plane integration which was found much more stable than on the real line. This technique can be used to calculate other spin-orbit influenced properties, such as anisotropy energy or spin-dependent spectroscopies.

Robust and accurate numerical methods were proposed to evaluate the Green function in the whole complex plane, and the smooth behavior of the cluster Green function for large imaginary energies was explained.

We saw that the EXAFS part of XMCD at the K-edge is simply connected to the spin-polarization of the p -states on the absorbing site. The high-energy part is therefore simpler to interpret than the near-edge part, where spin-orbit interactions with the neighbors gives strong contributions.

Our first application is encouraging, and further comparison with experiment, including the relation between magnetic and non-magnetic fine structure,⁴ will be presented in a forthcoming publication. Multiple-scattering calculation of XMCD at the $L_{II,III}$ -edges of Gd are presented in Refs. 83 and 37.

As observed by Ankudinov and Rehr,²⁰ XMCD in the x-ray range provides a very good test of effective potentials representing the exchange interaction of the photoelectron with matter. An alternative exchange potential was proposed by Zhogov et al.⁶³ in their treatment of magnetic EXAFS. In the present study, we have used the potential provided by the ground and relaxed-excited states, but did not include any specific exchange potential.

ACKNOWLEDGMENTS

We thank E. Dartyge, S. Pizzini, Ch. Giorgetti, F. Baudelet and A. Fontaine for providing us with the experimental spectra of bcc-Fe. We gratefully acknowledge the encouragement of G. B. White, who gave us detailed explanations of the mathematical framework. We thank also F. Gesztesy and B. Thaller for helpful discussions on the mathematical difficulties of the F-W Hamiltonian. We are very grateful to S. Hagenah, who suggested the contour integration to account for the Fermi energy, to J.J. Rehr for communication of his XMCD results prior to publication, to Ph. Sainctavit for his thorough reading of the manuscript, and to J. W. Wilkins for interesting discussions. One of us (Ch.B.) would like to thank K. H. Bennemann for his hospitality. This work was partly supported by NATO grant 9C93FR, by C.N.R.S. and by C.N.R.S.-NSF cooperative research program (Grant n° INT-9314455). M. A. acknowledges partial support provided by the Department of Energy (DOE) - Basic Energy Sciences, Division of Materials Sciences, and Supercomputer time provided by the Ohio Supercomputer.

APPENDIX: SYMMETRIZED BASIS

One of the advantages of the semi-relativistic limit of the Dirac Green function is that one is allowed to use the full local point symmetry of the absorbing atom without taking spin direction into account, since the spin and space functions are not coupled. In this section, we show how symmetrized bases were implemented to reduce the size of the problem.

For each spin state, the cluster potential is written as $V(\mathbf{r}) = \sum_i V^i(r_i)$ (i runs over atomic sites), and let P_a represent the action of the symmetry operation a on the cluster. If a belongs to the local point symmetry group \mathcal{G} of the absorbing atom ($i = 0$), then $P_a[V(\mathbf{r})] = V(\mathbf{r})$. Therefore, the Green function $G(z) = (z - H_0 - V)^{-1}$ is also invariant for operations of \mathcal{G} . This can be used to reduce the size of the multiple-scattering matrices.^{86,87}

In practice, we set up a symmetrized basis by the following procedure. For an irreducible

representation (irrep) α of the symmetry group, we take a matrix realization $\Gamma^{(\alpha)}$ of α , and we define the (pseudo-)projector:

$$P_{jj_0}^{(\alpha)\ell} = \frac{d_\alpha}{g} \sum_{a \in \mathcal{G}} \Gamma_{jj_0}^*(a) P^\ell(a) \quad (\text{A1})$$

where the cluster symmetry operator $P^\ell(a)$ has matrix elements in the $|n\ell m\rangle$ basis :

$$[P^\ell(a)]_{n'm'nm} = D_{m'm}^\ell(a) \delta_{n',a(n)}. \quad (\text{A2})$$

Here, g is the number of elements of the symmetry group \mathcal{G} , d_α is the dimension of irrep α , $D_{m'm}^\ell(a)$ is the (eventually improper) Wigner rotation matrix corresponding to the symmetry operation a of the point symmetry group \mathcal{G} .⁸⁸ We choose a column j_0 of the matrix realization ($j_0 = 1$) and, for each $|n\ell m\rangle$ representing a spherical harmonics Y_ℓ^m attached to site n , we calculate the projection $P_{j_0j_0}^{(\alpha)\ell} |n\ell m\rangle$. Let p be the set of atoms that can be obtained from a given atom by operations of \mathcal{G} . For each ℓ and each p one can generate a vector space $E(\alpha p \ell j_0)$ by calculating all the projections of $|n\ell m\rangle$, for $n \in p$ and $m = -\ell, \dots, \ell$. By singular value decomposition,⁶⁹ an orthonormal basis of $E(\alpha p \ell j_0)$ is obtained, which is denoted by $|\alpha p \ell j_0 s\rangle$, where $s = 1, \dots, \dim(E(\alpha p \ell j_0))$. This symmetrized basis can be written as a function of the initial basis kets :

$$|\alpha p \ell j_0 s\rangle = \sum_{\substack{n \in p \\ m = -\ell, \dots, \ell}} \langle n\ell m | \alpha p \ell j_0 s \rangle |n\ell m\rangle. \quad (\text{A3})$$

The partners of $|\alpha p \ell j_0 s\rangle$ are obtained by

$$|\alpha p \ell j s\rangle = P_{j_0j}^{(\alpha)\ell} |\alpha p \ell j_0 s\rangle \quad (\text{A4})$$

The symmetrized basis is then used to simplify the matrix inversion yielding the relevant multiple scattering matrix elements $\tau_{LL'}^{0i}$. It can be shown that

$$(P^\ell(a)H)_{nlm n'l'm'} = (HP^\ell(a))_{nlm n'l'm'} \quad (\text{A5})$$

Therefore,

$$\langle \alpha p \ell j s | H | \alpha' p' \ell' j' s' \rangle = \langle \alpha p \ell j_0 s | P_{j_0 j}^{(\alpha)\ell} H P_{j' j_0}^{(\alpha')\ell'} | \alpha' p' \ell' j'_0 s' \rangle \quad (\text{A6})$$

$$= \langle \alpha p \ell j_0 s | P_{j_0 j}^{(\alpha)\ell} P_{j' j_0}^{(\alpha')\ell} H | \alpha' p' \ell' j'_0 s' \rangle \quad (\text{A7})$$

$$= \delta_{\alpha, \alpha'} \delta_{j, j'} \langle \alpha p \ell j_0 s | H | \alpha' p' \ell' j'_0 s' \rangle. \quad (\text{A8})$$

Similarly, the atomic scattering matrix is diagonal:

$$\langle \alpha p \ell j s | T_a^{-1} | \alpha' p' \ell' j' s' \rangle = -\frac{\kappa}{t_\ell^p} \delta_{\ell, \ell'} \delta_{p, p'} \delta_{\alpha, \alpha'} \delta_{j, j'} \delta_{s, s'} \quad (\text{A9})$$

where $t_\ell^p = \sin \delta_\ell^p \exp(i\delta_\ell^p)$ and δ_ℓ^p is the ℓ -th phaseshift of the atoms of type p . Because of the transformation properties of matrices H and T_a , the full multiple-scattering matrix $\tau = [T_a^{-1} - \kappa H]^{-1}$ is diagonal in α and j :

$$\langle \alpha p \ell j s | \tau | \alpha' p' \ell' j' s' \rangle = \delta_{\alpha, \alpha'} \delta_{j, j'} \tau_{p \ell s p' \ell' s'}^{(\alpha)}. \quad (\text{A10})$$

In other words, the multiple-scattering matrix can be inverted separately for each irrep and it repeats itself $\dim(\Gamma^{(\alpha)})$ times in each irrep. For the example of a cluster of 259 Fe atoms, only the T_{1u} irrep is relevant, because of dipole selection rules, and the matrix to be inverted has dimension 288 instead of 4144. Once $\tau_{p \ell s p' \ell' s'}^{(\alpha)}$ is obtained, the matrix elements which are required for the calculation of XMCD at the K-edge are obtained through the basis change:

$$\tau_{1\epsilon \ell m}^{0i} = \sum_{\alpha j s s'} \langle 01\epsilon | \alpha p_0 1 j s \rangle \tau_{p_0 1 s p_i \ell s'}^{(\alpha)} \langle \alpha p_i \ell j s' | i \ell m \rangle \quad (\text{A11})$$

where p_i is the class of atoms to which atom i belongs.

An additional advantage of the use of a symmetrized basis is the fact that the inverse of τ is more rapidly calculated. In practice, the matrix elements $\langle \alpha p \ell j s | H | \alpha' p' \ell' j' s' \rangle$ must be calculated from the matrix elements $H_{\ell m \ell' m'}^{n n'}$ and the basis change matrix by

$$\langle \alpha p \ell j_0 s | H | \alpha' p' \ell' j'_0 s' \rangle = \sum_{\substack{n \in p \\ n' \in p'}} \sum_{m m'} \langle \alpha j_0 \ell p s | n \ell m \rangle H_{\ell m \ell' m'}^{n n'} \langle n' \ell' m' | \alpha j'_0 \ell' p' s' \rangle. \quad (\text{A12})$$

Instead of summing over all pairs $n \in p$ and $n' \in p'$, we can choose a member n_0 of class p , and a set of members n_1 of class p' which span all possible non-equivalent neighbors of n_0 in class p' . In other words, for each pair (n, n') , there is an element a of symmetry group \mathcal{G} and a representative n_1 such that $a(n) = n_0$ and $a(n') = n_1$. Therefore

$$H_{\ell m \ell' m'}^{n n'} = \sum_{\mu, \mu'} D_{\mu m}^{\ell *}(a) D_{\mu' m'}^{\ell}(a) H_{\ell \mu \ell' \mu'}^{n_0 n_1}. \quad (\text{A13})$$

We have also

$$\sum_m D_{\mu m}^{\ell}(a) \langle n \ell m | \alpha j_0 \ell p s \rangle = \sum_j \Gamma_{j_0 j}^{\alpha}(a^{-1}) \langle n_0 \ell \mu | \alpha j \ell p s \rangle, \quad (\text{A14})$$

which yields, using the fact that the symmetrized matrix elements of H do not depend on j_0 :

$$\langle \alpha p \ell j_0 s | H | \alpha p' \ell' j_0 s' \rangle = \frac{1}{d_{\alpha}} \sum_{j, j', j''} \sum_{n_1, a} \Gamma_{j'' j}^{\alpha}(a) \Gamma_{j'' j'}^{\alpha *}(a) \quad (\text{A15})$$

$$\times \sum_{m m'} \langle \alpha j \ell p s | n_0 \ell m \rangle H_{\ell m \ell' m'}^{n_0 n_1} \langle n_1 \ell' m' | \alpha j' \ell' p' s' \rangle. \quad (\text{A16})$$

From the orthogonality theorem of group representations,⁸⁷ the sum over j'' does not depend on a , and

$$\langle \alpha p \ell j_0 s | H | \alpha p' \ell' j_0 s' \rangle = \sum_{n_1, j} \frac{|p| N_{n_0 n_1}}{d_{\alpha}} \langle \alpha j \ell p s | n_0 \ell m \rangle H_{\ell m \ell' m'}^{n_0 n_1} \langle n_1 \ell' m' | \alpha j' \ell' p' s' \rangle, \quad (\text{A17})$$

where $|p|$ is the number of elements of class p , and $N_{n_0 n_1}$ is the number of elements n' of p' such that $a(n_0) = n_0$ and $a(n_1) = n'$, where $a \in \mathcal{G}$. Therefore, the sum is reduced to pairs of inequivalent neighbors.

From these symmetry considerations, one can show that, at the K-edge of a transition metal in a cubic environment, the spin-polarization of the d -shell of the absorbing atom cannot be measured, but the spin-polarization of the d -shell of the neighbors can. This was observed in the multiple-scattering approach in Refs. 4 and 50 and in the tight-binding approach in Ref. 78,79.

REFERENCES

- * Part of this work was carried out during a stay at the Institut für Theoretische Physik, Arnimallee 14, D-14195 Berlin.
- ¹ G. Schütz, W. Wagner, W. Wilhelm, P. Kienle, R. Zeller, R. Frahm, and G. Materlik, *Phys. Rev. Lett.* **58**, 737 (1987).
- ² Ch. Brouder and M. Hikam, *Phys. Rev. B* **43**, 3809 (1991).
- ³ For reviews, see F. Baudelet, Ch. Brouder, E. Dartyge, A. Fontaine, Ch. Giorgetti, G. Krill, J.-P. Kappler, and S. Pizzini, *Magnetic Multilayers*, Ed. L.H. Bennett and R.E. Watson, (World Scientific, Singapore, 1994), p.227-76; J. Stöhr and Y. Wu, *Proceedings of the NATO Advanced Study Institute "New Directions in Research with Third-Generation Soft X-Ray Synchrotron Radiation Sources"* Maratea, Italy, June 28- July 10, 1992, (Kluwer Academic Publishers, The Netherlands, 1994) p.221-50.
- ⁴ S. Pizzini, A. Fontaine, E. Dartyge, Ch. Giorgetti, F. Baudelet, J.-P. Kappler, P. Boher, and F. Giron, *Phys. Rev. B* **50**, 3779 (1994).
- ⁵ S. Pizzini, A. Fontaine, Ch. Giorgetti, E. Dartyge, J.-F. Bobo, M. Piecuch, F. Baudelet, *Proceedings of the 8th International Conference on X-ray Absorption Fine Structure*, Berlin, Germany, August 28 - Sept. 2, 1994, Eds. K. Baberschke and D. Arvanitis, *Physica B* **208-209**, 755 (1995)
- ⁶ H. Ebert, P. Strange, and B.L. Gyorffy, *Zeit. Phys. B* **73**, 77 (1988).
- ⁷ H. Ebert, P. Strange, and B.L. Gyorffy, *J. Appl. Phys.* **63**, 3055 (1988).
- ⁸ H. Ebert, P. Strange, and B.L. Gyorffy, *Proceedings of the International Conference on Magnetism* 25-29 July 1988, Paris, France, Ed. D. Givord, *J. Phys. (Paris)* **49** (C8), 31 (1988).
- ⁹ H. Ebert, B. Drittler, P. Strange, R. Zeller, and B.L. Gyorffy, *The effects of relativity in*

- atoms, molecules and the solid-state*, Ed. Wilson et al., (Plenum Press, New York, 1991) p.333-48.
- ¹⁰ H. Ebert and H. Akai, *Proceedings of the Symposium on Applications of Multiple Scattering Theory to Materials Science*, Boston, USA, 2-5 December 1991, Eds. W.H. Butler, P.H. Dederichs, A. Gonis and R.L. Weaver, Materials Research Society Symposium Proceedings, Vol. 253, p.329-40 (1992).
- ¹¹ S. Stähler, G. Schütz, and H. Ebert, Phys. Rev. B **47**, 818 (1993).
- ¹² H.J. Gotsis and P. Strange, J. Phys.: Condens. Matter **6**, 1409 (1994).
- ¹³ P. Strange and B.L. Gyorffy, J. Phys.: Condens. Matter **2**, 9451 (1990).
- ¹⁴ H. Ebert, H. Akai, H. Maruyama, A. Koizumi, H. Yamazaki, and G. Schütz, *Proceedings of the International Conference on the Physics of Transition Metals* Darmstadt, Germany, 20-24 July 1992, Eds. P.M. Oppeneer and J. Kübler, Int. J. Mod. Phys. B **7**, 750 (1993).
- ¹⁵ H. Ebert, *Proceedings of the 7th International Conference on X-ray Absorption Fine Structure*, Kobe, Japan, 23-29 August 1992, Eds. H. Kuroda, T. Ohta, T. Murata, Y. Udagawa and M. Nomura, Jpn. J. Appl. Phys. **32** (Suppl. 32-2), 299 (1993).
- ¹⁶ H.J. Gotsis, P. Strange, and J.B. Staunton, Solid State Commun. **92**, 449 (1994).
- ¹⁷ J.C. Lang, Xindong Wang, V.P. Antropov, B.N. Harmon, A.I. Goldman, H. Wan, G.C. Hadjipanayis, and K.D. Finkelstein, Phys. Rev. B **49**, 5993 (1994).
- ¹⁸ P. Strange, E. Arola, B.L. Gyorffy, *Proceedings of the International Conference on Magnetism*, Warsaw, Poland, 22-26 August 1994, Eds. R. Troć, J. Morkowski and H. Szymczak, J. Magn. Magn. Mat. **140-144**, 73 (1995).
- ¹⁹ H. Ebert, *Spin-orbit influenced spectroscopies of magnetic solids*, Eds. H. Ebert and G. Schütz, Lecture Notes in Physics Vol.**466** Springer, Berlin, (1996), p.159-77.
- ²⁰ A. Ankudinov and J.J. Rehr, Phys. Rev. B **52**, 10214 (1995).

- ²¹ U. von Barth and G. Grossman Phys. Rev. B **25**, 5150 (1982), U. von Barth and G. Grossman, Phys. Scripta **28**, 107 (1983).
- ²² M. Alouani, J. M. Koch, and M. A. Khan, Solid State Comm. **60** , 657 (1986).
- ²³ M. Alouani, Phys. Rev. B **49**, 16038 (1994).
- ²⁴ O. K. Andersen, Phys. Rev. B **12**, 3060 (1975).
- ²⁵ L.L. Foldy and S.A. Wouthuysen, Phys. Rev. **78**, 29 (1950).
- ²⁶ J.D. Morrison and R.E. Moss, Molecular Physics **41**, 491 (1980).
- ²⁷ F. Gesztesy, H. Grosse, and B. Thaller, Ann. Inst. Henri Poincaré **40**, 159 (1984).
- ²⁸ F. Gesztesy, H. Grosse, and B. Thaller, Adv. Appl. Math. **6**, 159 (1985).
- ²⁹ S. Nagano, Phys. Rev. B **50**, 7962 (1994).
- ³⁰ F. Gesztesy, H. Grosse, and B. Thaller, Phys. Lett. B **116**, 155 (1982).
- ³¹ T. Udim, Arch. Math. **38**, 357 (1982).
- ³² B. Thaller, private communication.
- ³³ W. Hunziker, Helv. Phys. Acta **61**, 257 (1988).
- ³⁴ W. Kutzelnigg, E. Ottschofski, and R. Franke, J. Chem. Phys. **102**, 1740 (1995).
- ³⁵ A.J. Sadlej, J.G. Snijders, E. van Lenthe, and E.J. Baerends, J. Chem. Phys. **102**, 1758 (1995).
- ³⁶ C.R. Natoli, *Proceedings of the 8th International Conference on X-ray Absorption Fine Structure*, Berlin, Germany, August 28 - Sept. 2, 1994, Eds. K. Baberschke and D. Arvanitis, Physica B **208-209**, 5 (1995).
- ³⁷ Ch. Brouder, *Synchrotron Radiation and Magnetism*, (Editions de Physique, Paris, 1996).
- ³⁸ B. Thaller, *The Dirac Equation* (Springer, Berlin, 1992).

- ³⁹ G.B. White, *Ann. Inst. Henri Poincaré* **59**, 269 (1993).
- ⁴⁰ A. Arai, *Integr. Equat. Oper. Th.* **21**, 139 (1995).
- ⁴¹ G.B. White, private communication.
- ⁴² M. Morin, D.R. Salahub, S. Nour, C. Mehadji, and H. Chermette, *Chem. Phys. Lett.* **159**, 472 (1989).
- ⁴³ A.C. Jenkins and P. Strange, *J. Phys.: Condens. Matter* **6**, 3499 (1994).
- ⁴⁴ A.C. Jenkins and P. Strange, *Proceedings of the International Conference on Magnetism*, Warsaw, Poland, 22-26 August 1994, Eds. R. Troć, J. Morkowski and H. Szymczak, *J. Magn. Magn. Mat.* **140-144**, 37 (1995).
- ⁴⁵ T.A. Tyson, *Phys. Rev. B* **49**, 12578 (1994).
- ⁴⁶ Y. Jeon, J. Chen, and M. Croft, *Phys. Rev. B* **50**, 6555 (1994).
- ⁴⁷ J. Desclaux, *Comput. Phys. Commun.* **9**, 31 (1975).
- ⁴⁸ F. Gesztesy, B. Thaller, and H. Grosse, *Phys. Rev. Lett.* **50**, 625 (1983).
- ⁴⁹ R.D. Cowan, *The Theory of Atomic Structure and Spectra* (University of California Press, Berkeley, 1981).
- ⁵⁰ M. Hikam, *Ph. D. Thesis*, University of Nancy, 1992.
- ⁵¹ R.V. Vedrinskiy and A.A. Novakovich, *Phys. Metals Metallogr.* **39**, 1 (1975).
- ⁵² W. Bulla, F. Gesztesy, and K. Unterkofler, *Lett. Math. Phys.* **15**, 313 (1988).
- ⁵³ S. Agmon and M. Klein, *Duke Math. J.* **68**, 337 (1992).
- ⁵⁴ Ph. Saintavit, *Ph.D. Thesis*, University of Paris VI.
- ⁵⁵ R.G Newton, *Scattering Theory of Waves and Particles*, second edition, Springer, New-York, 1982, p.177.

- ⁵⁶ C.R. Natoli, private communication.
- ⁵⁷ H. Dreyssé and R. Riedinger, *J. Physique* **42** 437 (1982); R. Zeller, J. Deutz, and P.H. Dederichs, *Solid State Commun.* **44** 993 (1982); R.V. Vedrinskii, V.L. Kraizman, A.A. Novakovich and V.Sh. Machavariani, *J. Phys.: Condens. Matter* **4** 6155 (1992).
- ⁵⁸ F.W. Byron and R.W. Fuller, *Mathematics of classical and quantum physics* (Addison-Wesley, Reading, 1970).
- ⁵⁹ This can be shown from the inequality $|G(z)| \leq 1/d(z, \Sigma)$, where $d(z, \Sigma)$ is the distance between z and the spectrum of H . If E_0 is the energy of the 1s state, $d(z, \Sigma) \geq \max(E_0 - \text{Re}z, |\text{Im}z|)$.
- ⁶⁰ Using the distribution identity $1/(x+i\epsilon) = P(1/x) - i\pi \text{sgn}(\epsilon)\delta(x)$, where P is the principal-value symbol and $\epsilon = E - E_F$, one can show that as E tends towards E_F with either $E > E_F$ or $E < E_F$, the value of the right-hand side of Eq. (14) converges to $(1/2)\text{Im}[(E + i\Gamma - E_i)G(E + i\Gamma)] - (\Gamma/\pi)P \int_0^\infty dt \text{Re}[(E_F + it - E_i)G(E_F + it)]/(t^2 - \Gamma^2)$. Efficient algorithms exist to calculate principal value integrals (e.g. A. Natarajan and N. Mohankumar, *J. Comput. Phys.* **116**, 365 (1995), K. Diethelm, *J. Comp. Appl. Math.* **56**, 321 (1994) and J.A.C. Weidman, *Math. Comp.*, **64** 745 (1995)).
- ⁶¹ J.J. Rehr, *Jpn. J. Appl. Phys.* **32**, Suppl. **32-2**, 8 (1993).
- ⁶² Ch. Brouder, *Proceedings of the Symposium on Applications of Multiple Scattering Theory to Materials Science*, Boston, USA, 2-5 December 1991, Materials Research Society Symposium Proceedings, Vol. 253, (1992) p.411.
- ⁶³ S.A. Zhogov, V.N. Lavruk, and V.M. Matveev, *Proceedings of the International Conference on Magnetism*, Warsaw, Poland, 22-26 August 1994, Eds. R. Troć, J. Morkowski and H. Szymczak, *J. Magn. Magn. Mat.* **140-144**, 1197 (1995).
- ⁶⁴ G.A. Mulhollan, Xia Zhang, F.B. Dunning, and G.K. Walters, *Phys. Rev. B* **41**, 8122 (1990).

- ⁶⁵ B.L. Gyorffy and M.J. Stott, in *Band Structure Spectroscopy of Metals and Alloys*, Eds. D.J. Fabian and L.M. Watson (Academic Press, London, 1973), p.385-403.
- ⁶⁶ M. Abramowitz and I.A. Stegun, *Handbook of Mathematical Functions*, 9th ed. (Dover, New York, 1965).
- ⁶⁷ J.R. Taylor, *Scattering Theory: The quantum theory on nonrelativistic collisions* (Wiley, New York, 1972).
- ⁶⁸ A.G. Koures and F.E. Harris, *J. Chem. Phys.* **89**, 7344 (1988).
- ⁶⁹ W.H. Press, B.P. Flannery, S.A. Teukolsky, and W.T. Vetterling, *Numerical Recipes* (Cambridge University Press, Cambridge, 1986).
- ⁷⁰ and because the signs of the last two terms of Eq. (62) in Ref. 2 are wrong.
- ⁷¹ M. Reed and B. Simon, *Methods of modern mathematical physics, Vol.III. Scattering theory* (Academic Press, New York, 1979).
- ⁷² J.J. Rehr and R.C. Albers, *Phys. Rev. B* **41**, 8139 (1990).
- ⁷³ F. Manar and Ch. Brouder, *Proceedings of the 8th International Conference on X-ray Absorption Fine Structure*, Berlin, Germany, August 28 - Sept. 2, 1994, Eds. K. Baberschke and D. Arvanitis, *Physica B* **208-209**, 79 (1995) and D. Sébilleau, *J. Phys.: Condens. Matter* **7**, 6211 (1995).
- ⁷⁴ R.W. Freund, *SIAM J. Sci. Stat. Comput.* **13**, 425 (1992).
- ⁷⁵ D.A. Case and C.Y. Yang, *Int. J. Quant. Chem.* **18**, 1091 (1980).
- ⁷⁶ U. von Barth and L. Hedin, *J. Phys. C* **5**, 1629 (1972).
- ⁷⁷ O. Jepsen and O. K. Andersen, *Solid State Commun.* **9**, 1763 (1971); G. Lehmann and M. Taut, *Phys. Stat. Sol.* **54**, 469 (1972).
- ⁷⁸ J. Igarashi and K. Hirai, *Phys. Rev. B* **50**, 17820 (1994).

- ⁷⁹ J. Igarashi and K. Hirai, Phys. Rev. B **53**, 6442 (1996).
- ⁸⁰ T.A. Tyson, K.O. Hodgson, C.R. Natoli, and M. Benfatto, Phys. Rev. B **46**, 5997 (1992).
- ⁸¹ Ch. Brouder, M.F. Ruiz López, R.F. Pettifer, M. Benfatto, and C.R. Natoli, Phys. Rev. B **39**, 1488 (1989).
- ⁸² E. Dartyge, A. Fontaine, Ch. Giorgetti, S. Pizzini, F. Baudelet, G. Krill, Ch. Brouder, and J.-P. Kappler, Phys. Rev. B **46**, 3155 (1992) and E. Dartyge, F. Baudelet, Ch. Brouder, A. Fontaine, Ch. Giorgetti, J.-P. Kappler, G. Krill, M.F. Lopez, S. Pizzini, *Proceedings of the 8th International Conference on X-ray Absorption Fine Structure*, Berlin, Germany, August 28 - Sept. 2, 1994, Eds. K. Baberschke and D. Arvanitis, Physica B **208-209**, p.751-4 (1995) and M. Knülle, D. Ahlers and G. Schütz, Solid State Commun. **94**, 267 (1995).
- ⁸³ Ch. Brouder, M. Alouani, Ch. Giorgetti, E. Dartyge and F. Baudelet, *Spin-orbit influenced spectroscopies of magnetic solids*, Lecture Notes in Physics Vol.**466** (Springer, Berlin, 1996), p.259-74.
- ⁸⁴ I. Harada and A. Kotani, J. Phys. Soc. Jpn **63**, 1285 (1994).
- ⁸⁵ M. Verdaguer, T. Mallah, C. Hélyary, F. L'Hermite, Ph. Sainctavit, M.-A. Arrio, D. Babel, F. Baudelet, E. Dartyge, A. Fontaine, Physica B **208-209**, 765 (1995).
- ⁸⁶ J.B. Diamond, Chem. Phys. Lett. **20**, 63 (1973).
- ⁸⁷ W. Ludwig and C. Falter, *Symmetries in Physics* (Springer, Berlin, 1988).
- ⁸⁸ L.C. Biedenharn and J.D. Louck, *Angular Momentum in Quantum Physics* (Addison-Wesley, Reading, 1981).

FIGURES

FIG. 1. Calculated K-edge absorption spectrum (thick line) and x-ray magnetic circular dichroism (thin line) of a cluster of 259 atoms of bcc-Fe near the singularity at the vicinity of Fermi level.

FIG. 2. Pole structure of the integrand in the second term of Eq. (12).

FIG. 3. (a) : $\sum_s \tilde{\sigma}_{0a}^s + \tilde{\sigma}_{0n}^s$ and (b) : $\sum_s (-1)^{s-1/2} \tilde{\sigma}_{1a}^s + \tilde{\sigma}_{1l}^s + \tilde{\sigma}_{1n}^s$ for complex energies along the line $E_F + it$ ($E_F = 0$). In each case, the corresponding atomic quantities $\sum_s \tilde{\sigma}_{0a}^s$ and $\sum_s (-1)^{s-1/2} \tilde{\sigma}_{1a}^s$ are plotted, to show the convergence of the full Green function to the atomic Green function.

FIG. 4. Calculated (a) K-edge absorption spectrum and (b) x-ray magnetic circular dichroism (XMCD) of a cluster of 259 atoms of bcc-Fe with different values of Fermi level, $E_F = -\infty, -2, 0, 2$ eV. For the XMCD signal, the size of the first positive structure depends strongly on the position of Fermi level, and disappears for E_F above 2 eV.

FIG. 5. Comparison of the calculated (a) K-edge absorption spectrum and (b) the x-ray magnetic circular dichroism (XMCD) of a cluster of 259 atoms of bcc-Fe with the experimental results of Ref. 4 The Fermi level is $E_F=0$ eV.

FIG. 6. Contribution to $\tilde{\sigma}_{1n}$ of the absorbing site and the first two shells (from top to bottom) and for $\ell=1,2,3$. No Fermi energy was used. The contribution of a given shell is the contribution of one atom of the shell multiplied by the number of atoms in the shell.

FIG. 7. Calculated (a) K-edge absorption spectrum and (b) x-ray magnetic circular dichroism (XMCD) of a cluster of 259 atoms of bcc-Fe with (thick line) and without (thin line) core hole.

FIG. 8. Comparison of the calculated (a) K-edge absorption spectrum and (b) x-ray magnetic circular dichroism (XMCD) of a cluster of 51 atoms of bcc-Fe with the experimental results of Ref. 4. The Fermi level is $E_F=0$ eV, the core-hole broadening is $\Gamma = 2$ eV, and the maximum scattering wave is $\ell_{\max}=8$.

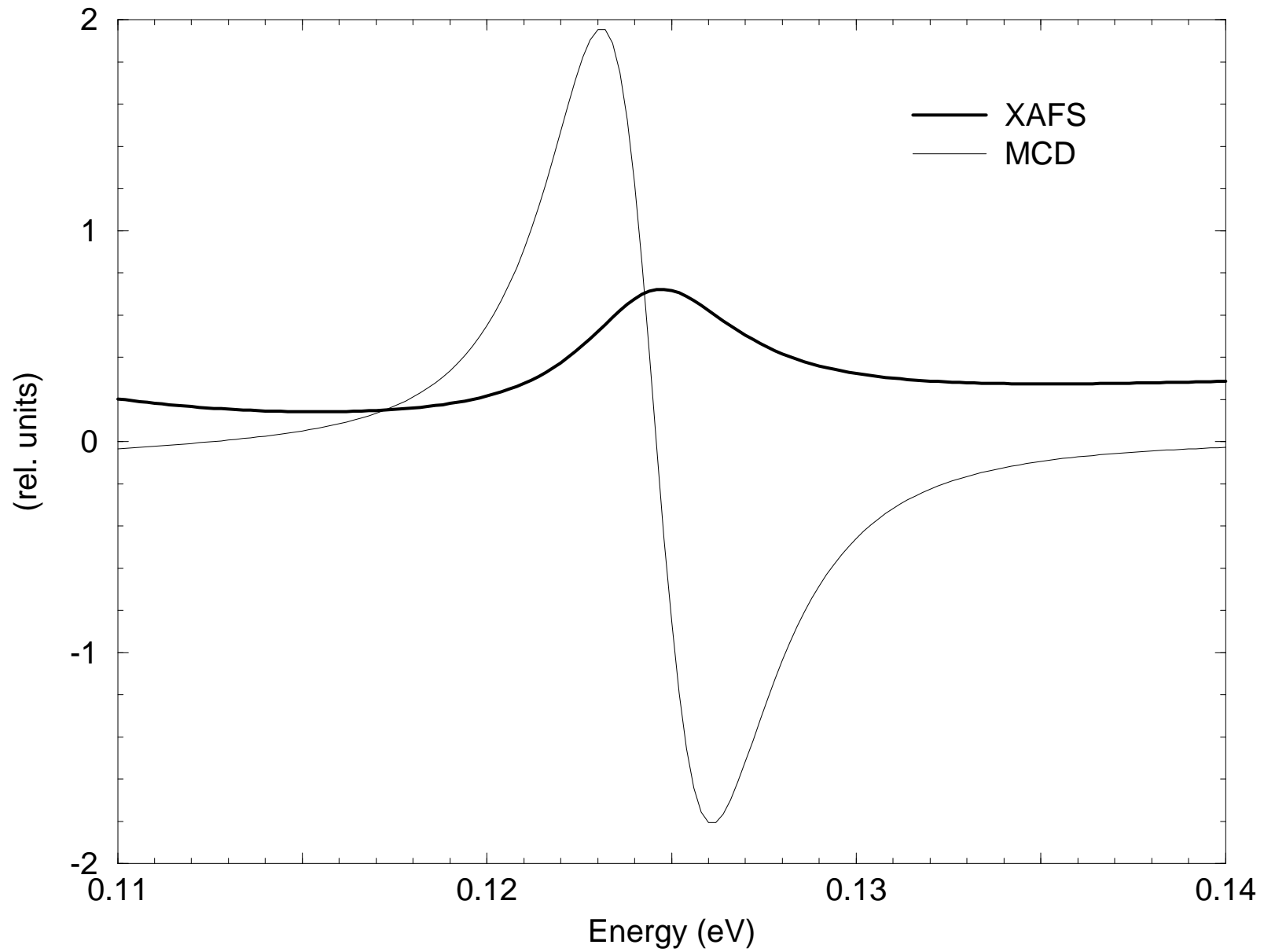
FIG. 9. (a) Comparison of the calculated K-edge absorption spectrum with the density of p states projected on the absorbing atom and (b) comparison of the calculated XMCD with the spin polarization of the density of p states projected on the absorbing atom. The derivative of the DOS is also presented, to illustrate the rigid band picture that becomes valid at high energy.

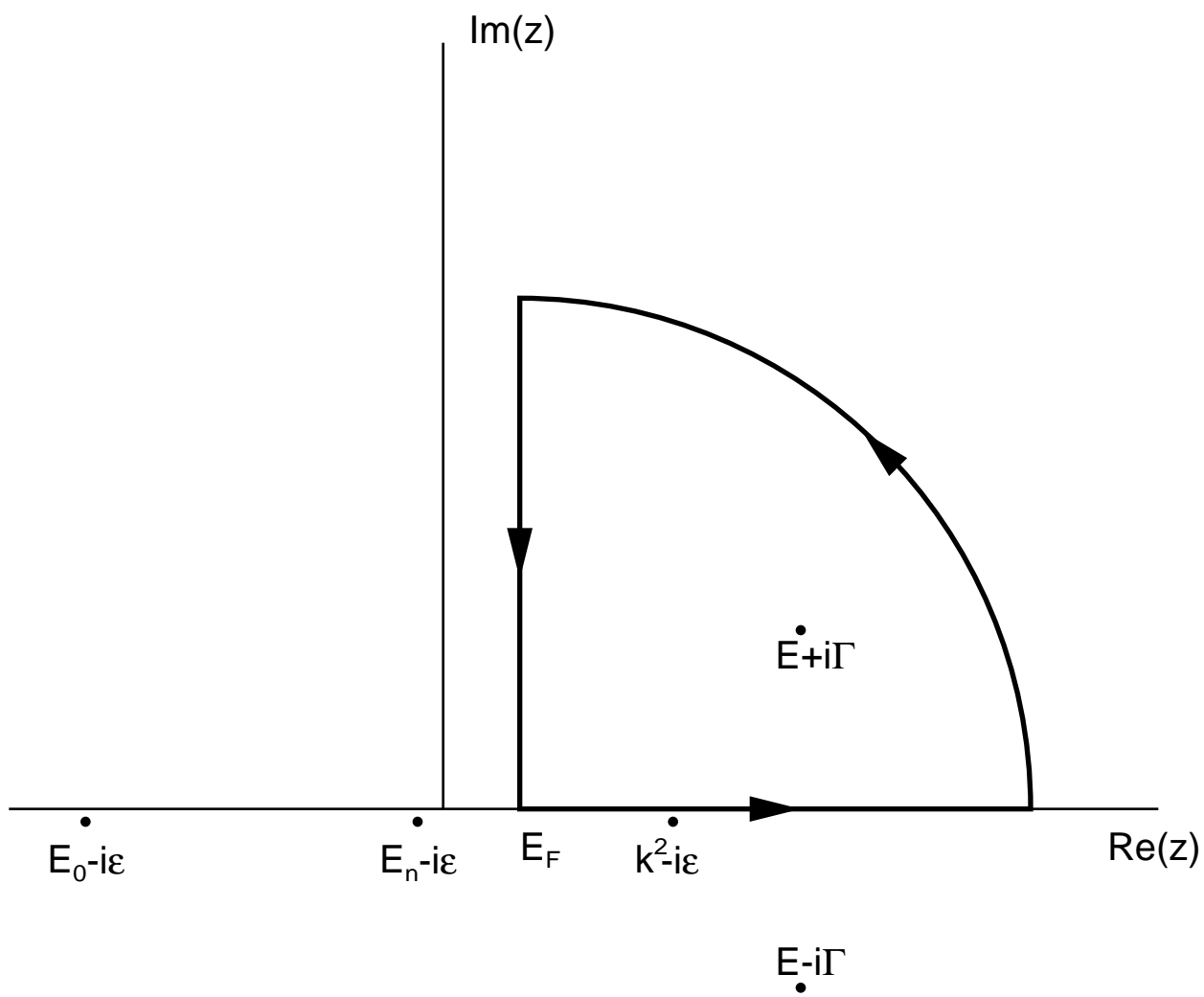
FIG. 10. Comparison of the XMCD spectrum with the second derivative of the absorption spectrum (multiplied by 10) for a cluster of 51 iron atoms.

FIG. 11. (a) Comparison of the calculated K-edge absorption spectrum with the single and double scattering expansion (b) comparison of the calculated XMCD with the single and double scattering expansion.

Divergence at real energies

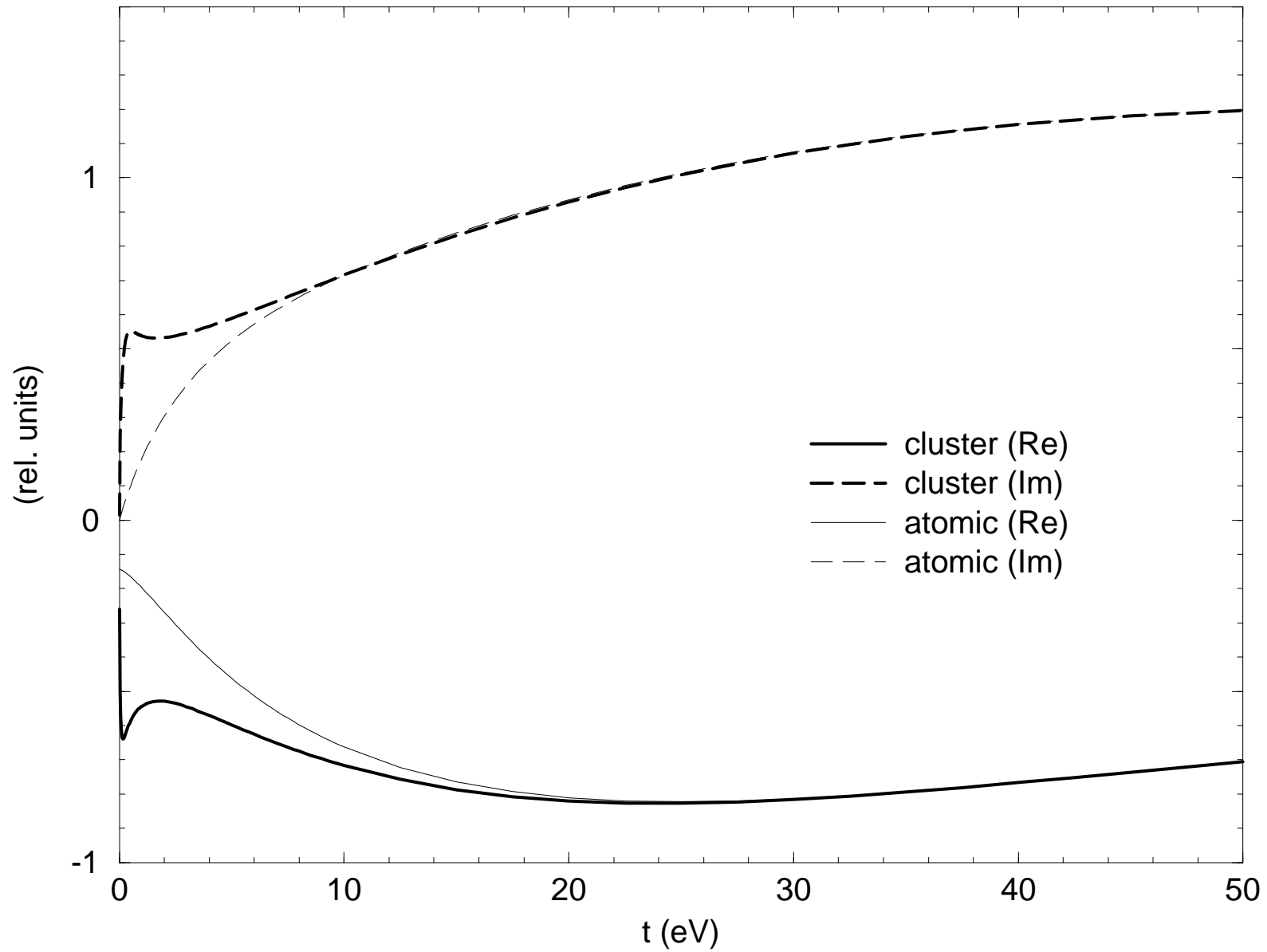
bcc-Fe 259 atoms $l=3$





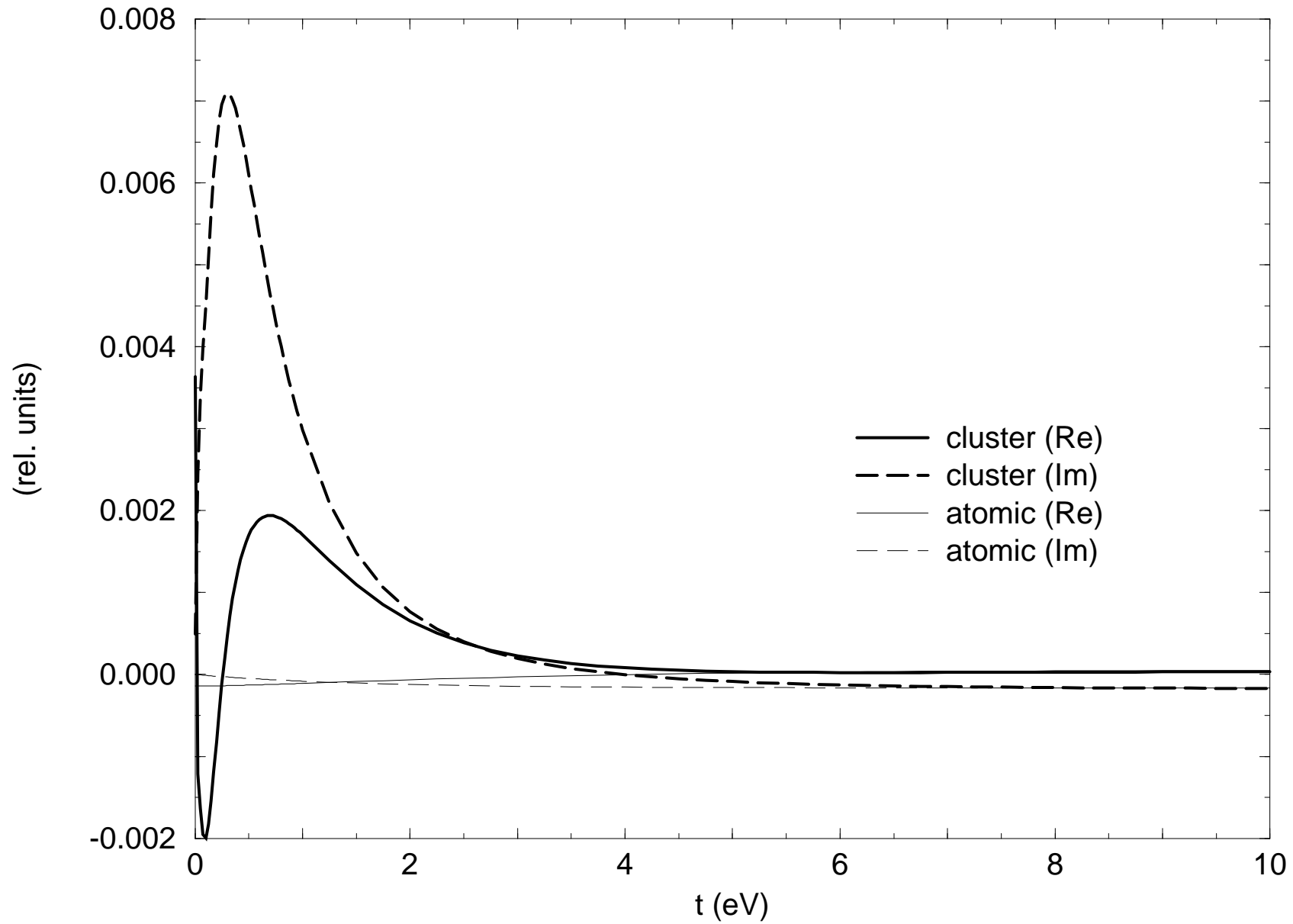
$\sigma_0(z)$ for $z=E_f+it$

$E_f=0\text{eV}$ bcc-Fe 259 atoms $l=3$



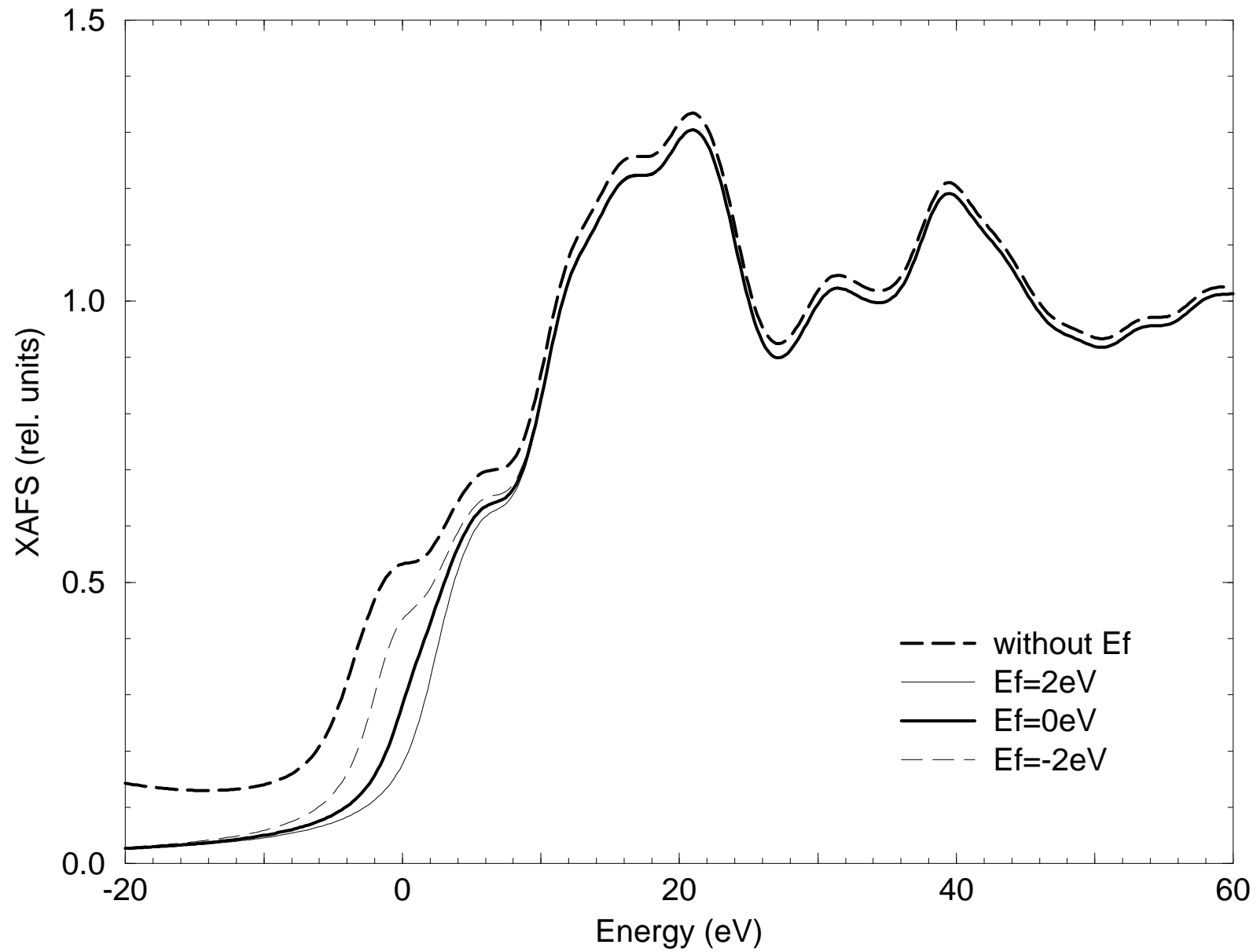
sigma1(z) for z=Ef+it

Ef=0eV bcc-Fe 259 atoms l=3



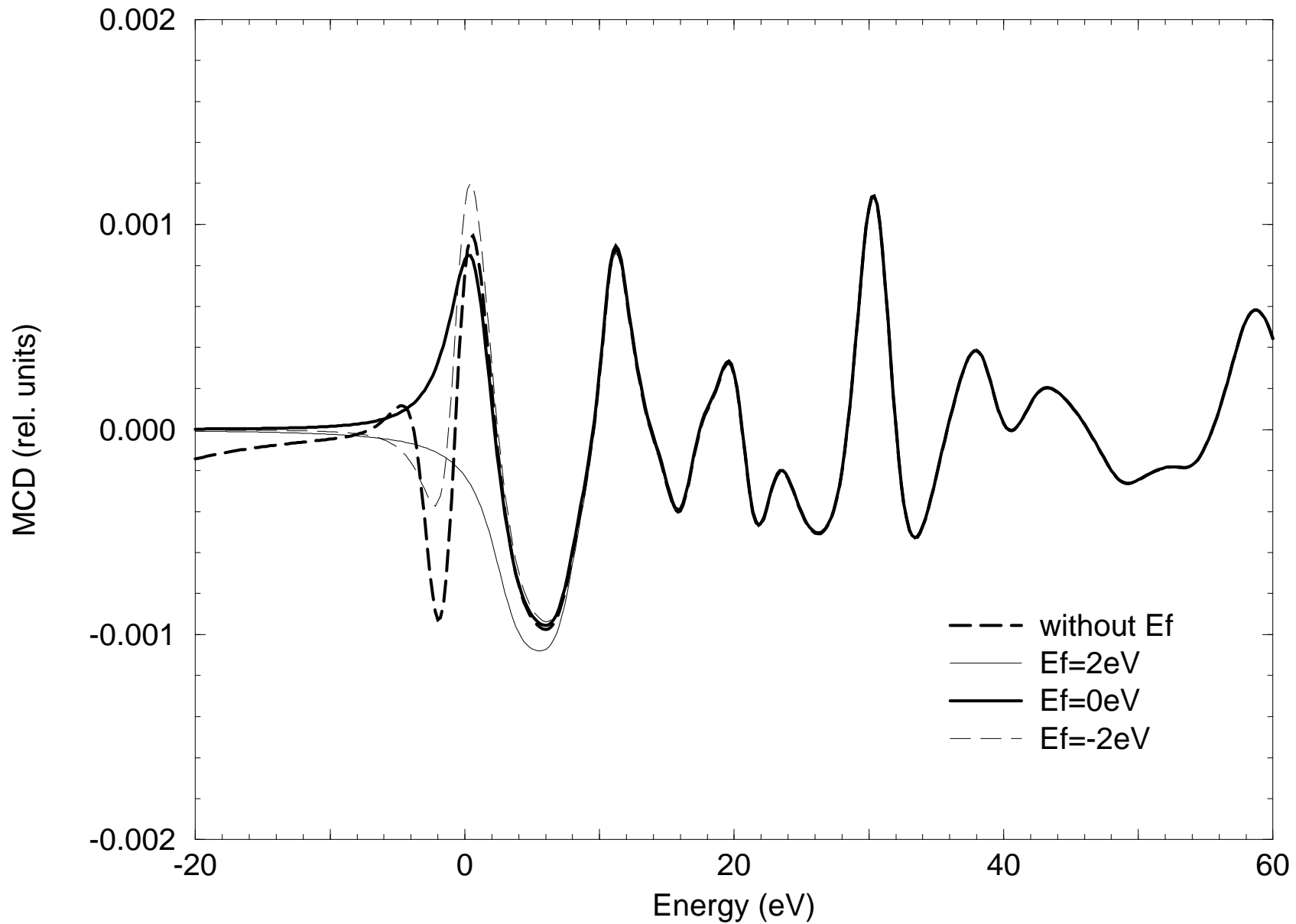
Influence of Fermi energy

bcc-Fe 259 atoms $l=3$



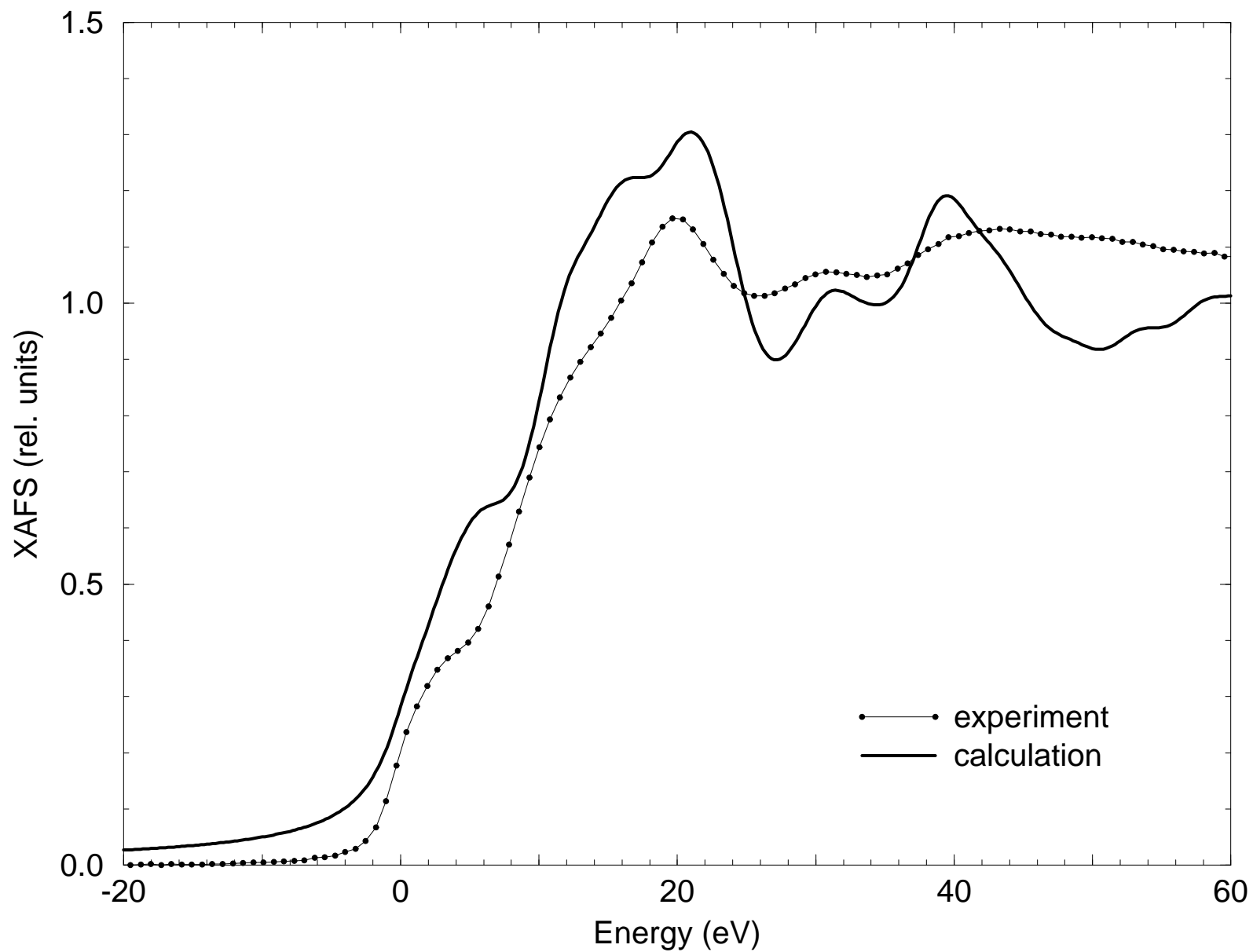
Influence of Fermi energy

bcc-Fe 259 atoms $l=3$



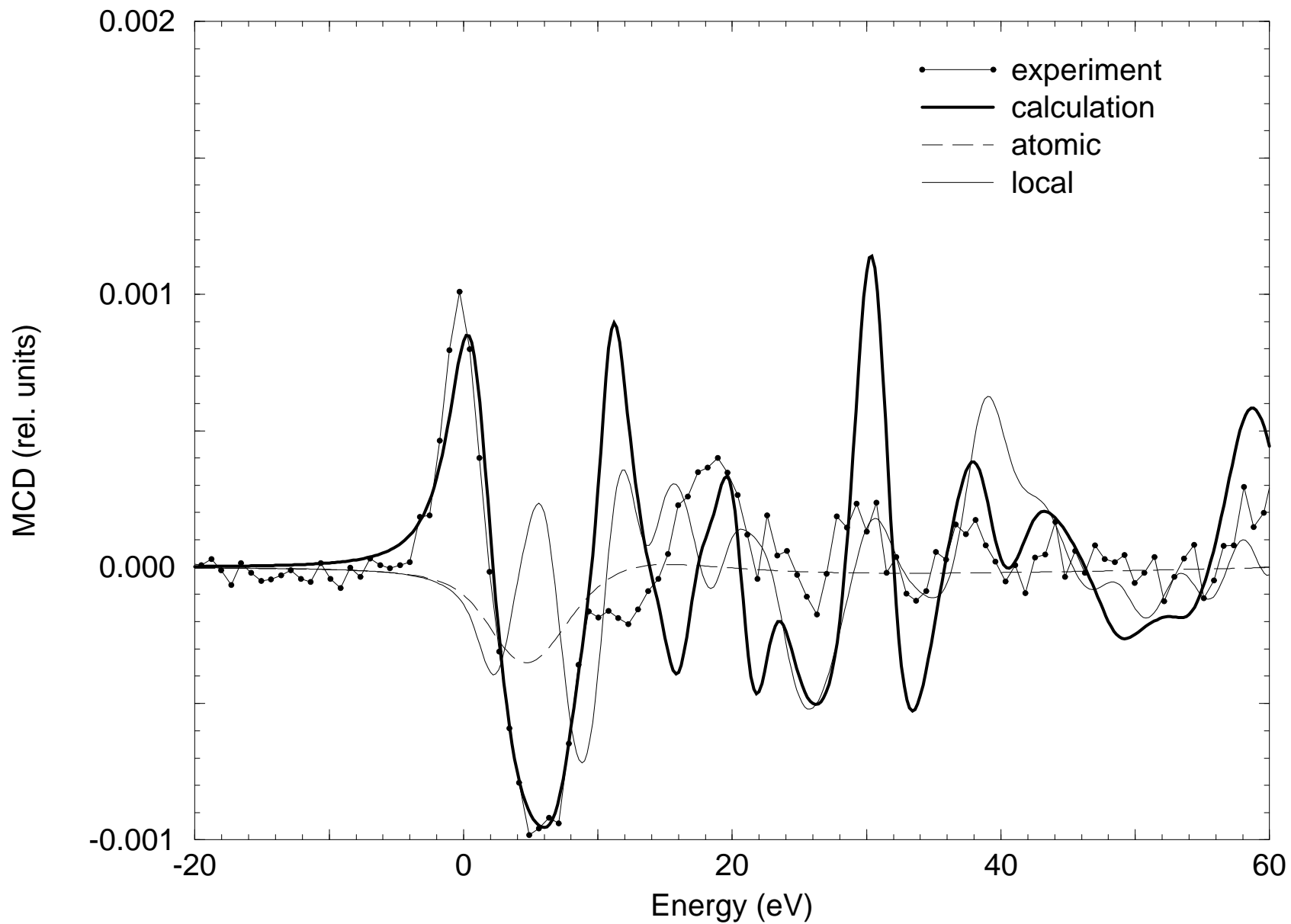
Calculation vs experiment

bcc-Fe 259 atoms $l=3$



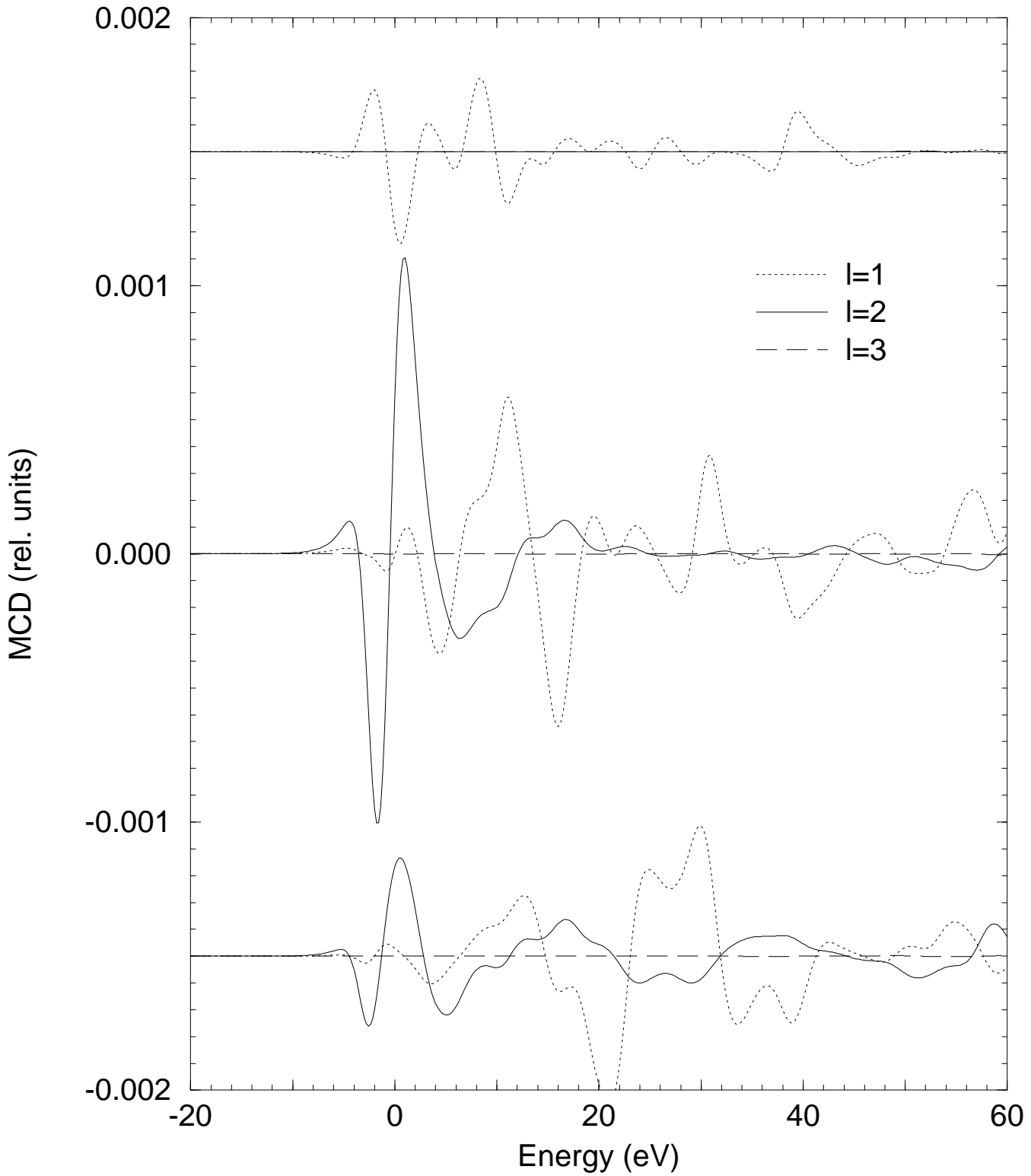
Calculation vs experiment

bcc-Fe 259 atoms $l=3$



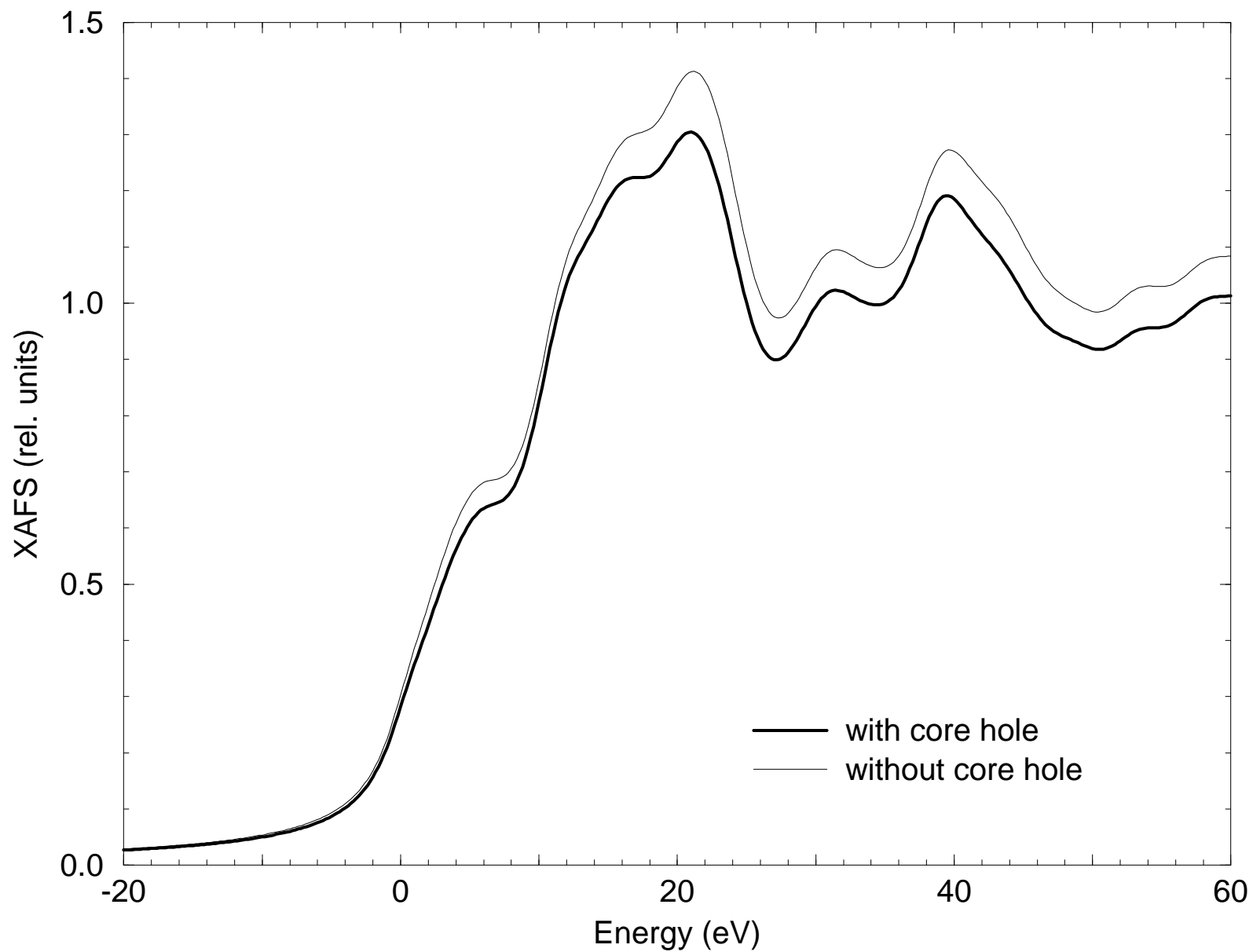
Neighbor terms

bcc-Fe 259 atoms $l=3$



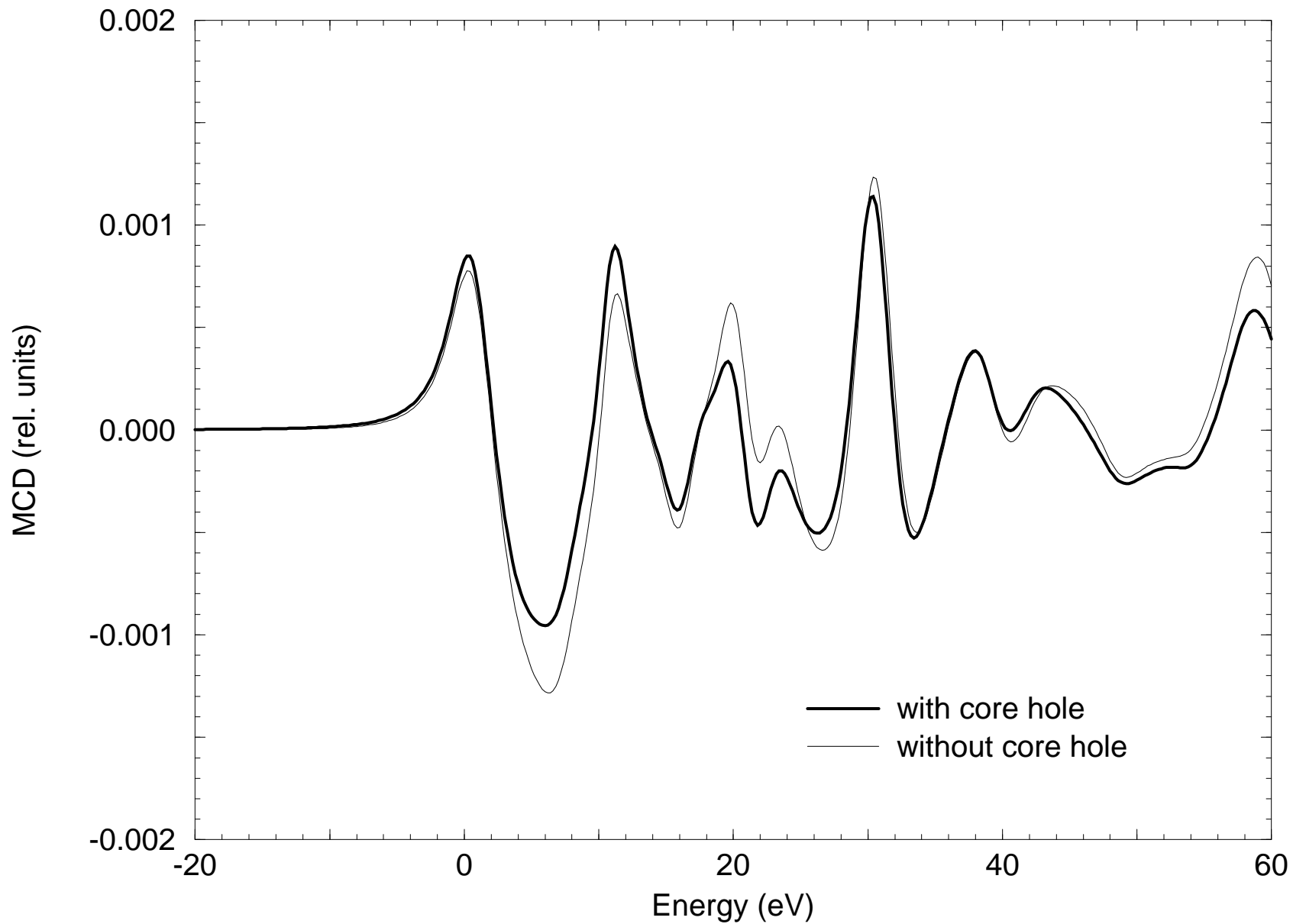
Core hole effect

bcc-Fe 259 atoms $l=3$ $E_f=0$



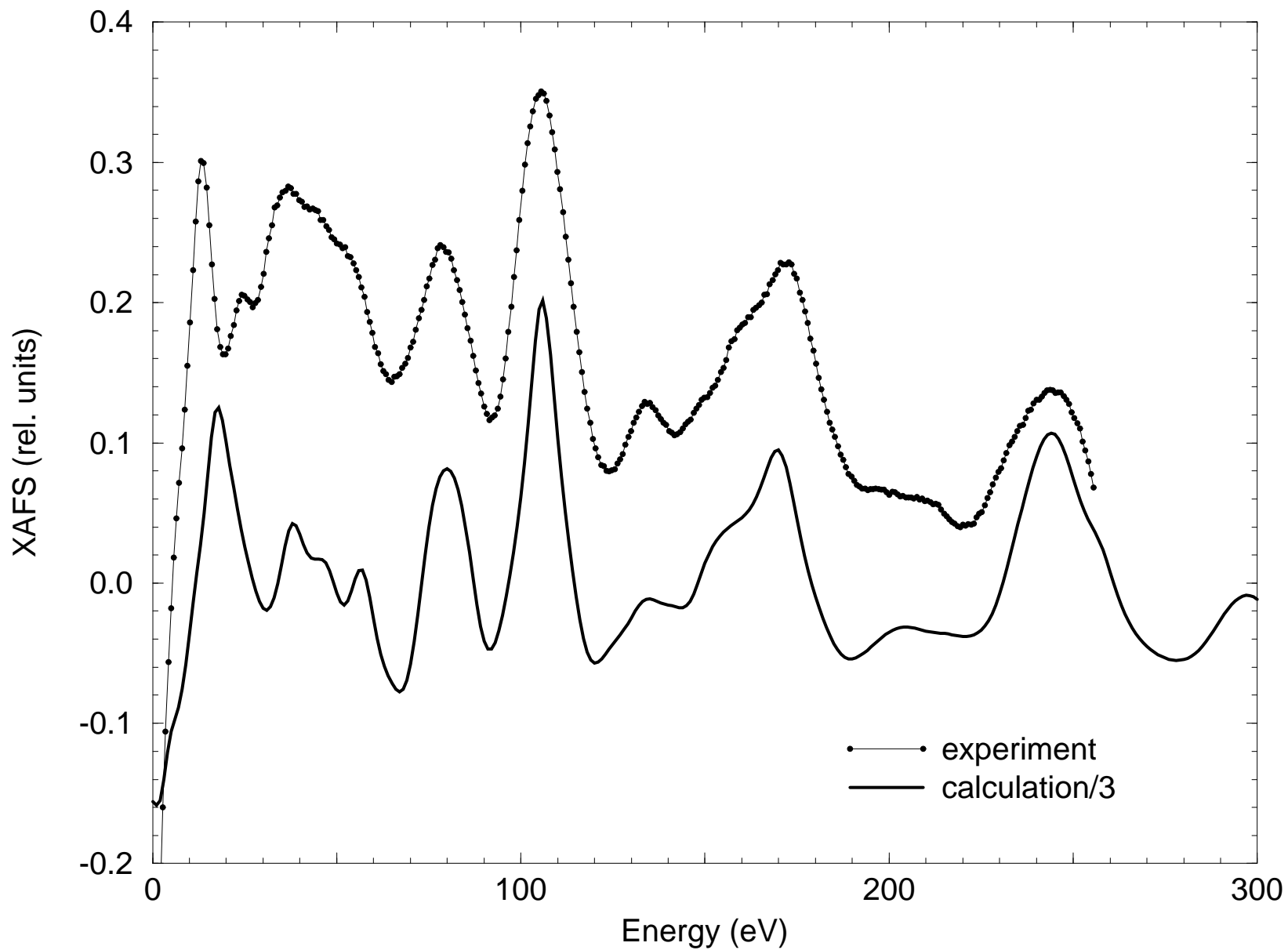
Core hole effect

bcc-Fe 259 atoms $l=3$ $E_f=0$



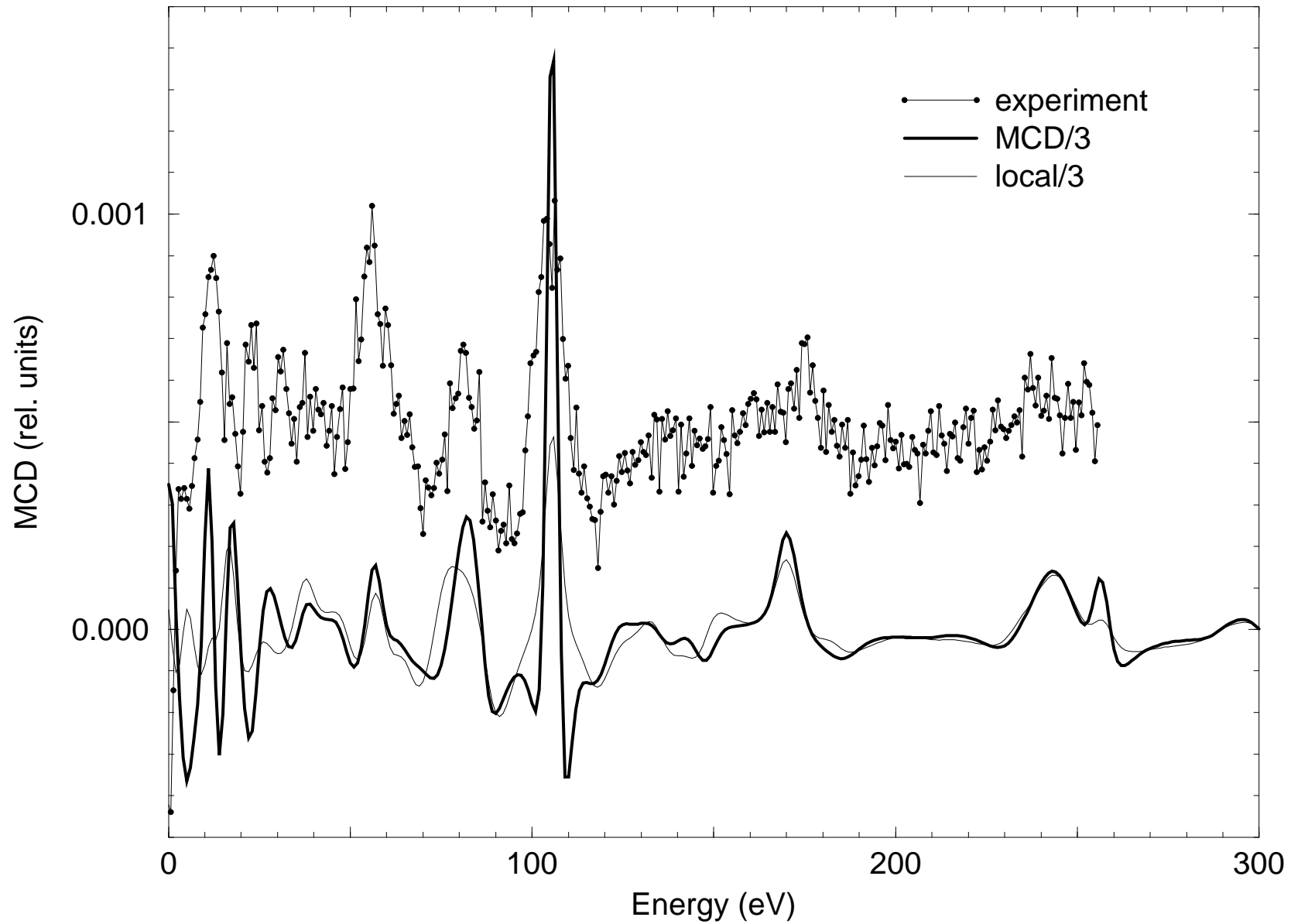
Calculation vs experiment : XAFS

bcc-Fe 51 atoms l=8



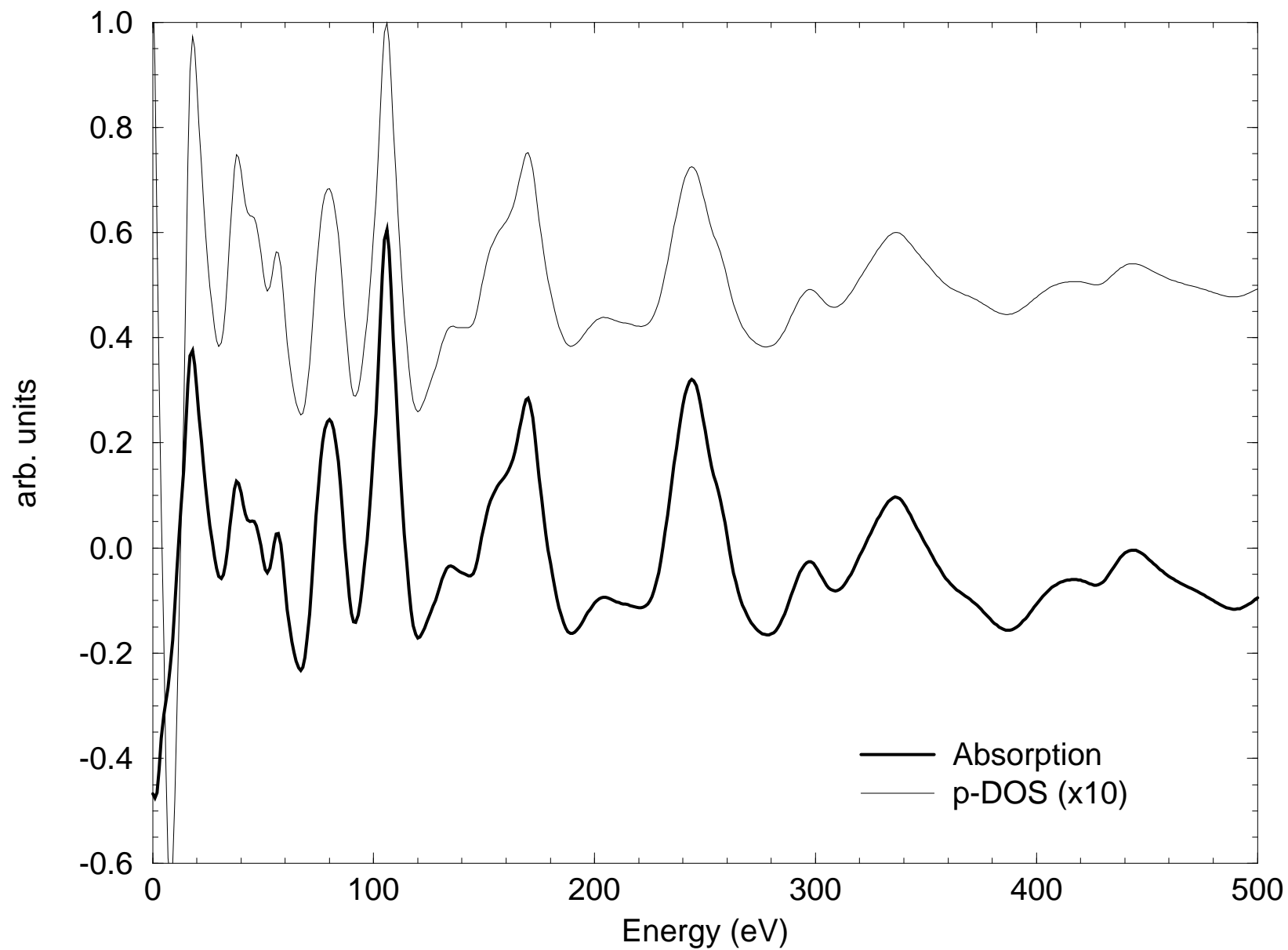
Calculation vs experiment : MCD

bcc-Fe 51 atoms $l=8$



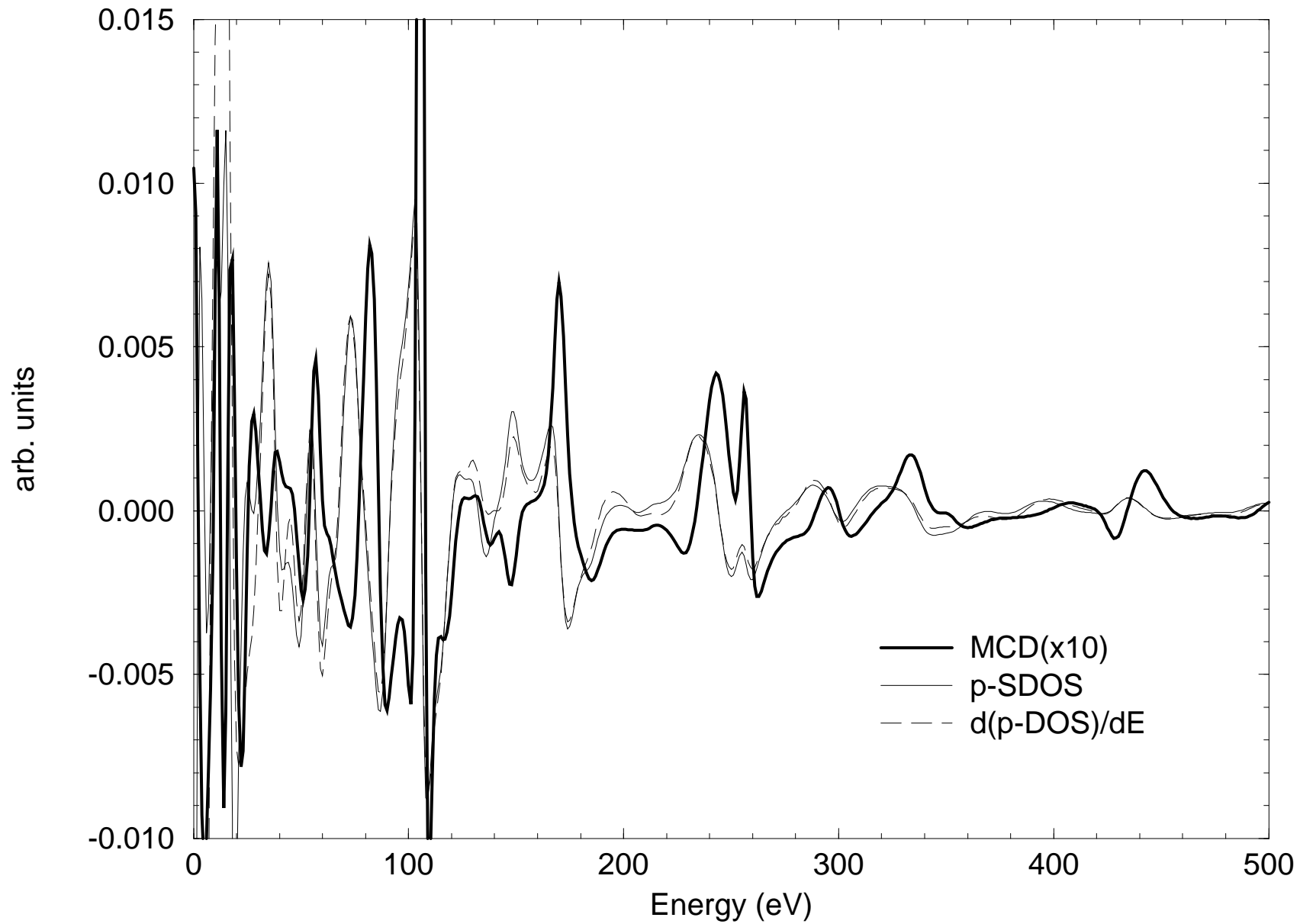
p-DOS vs absorption

Fe bcc 51 atoms l=8



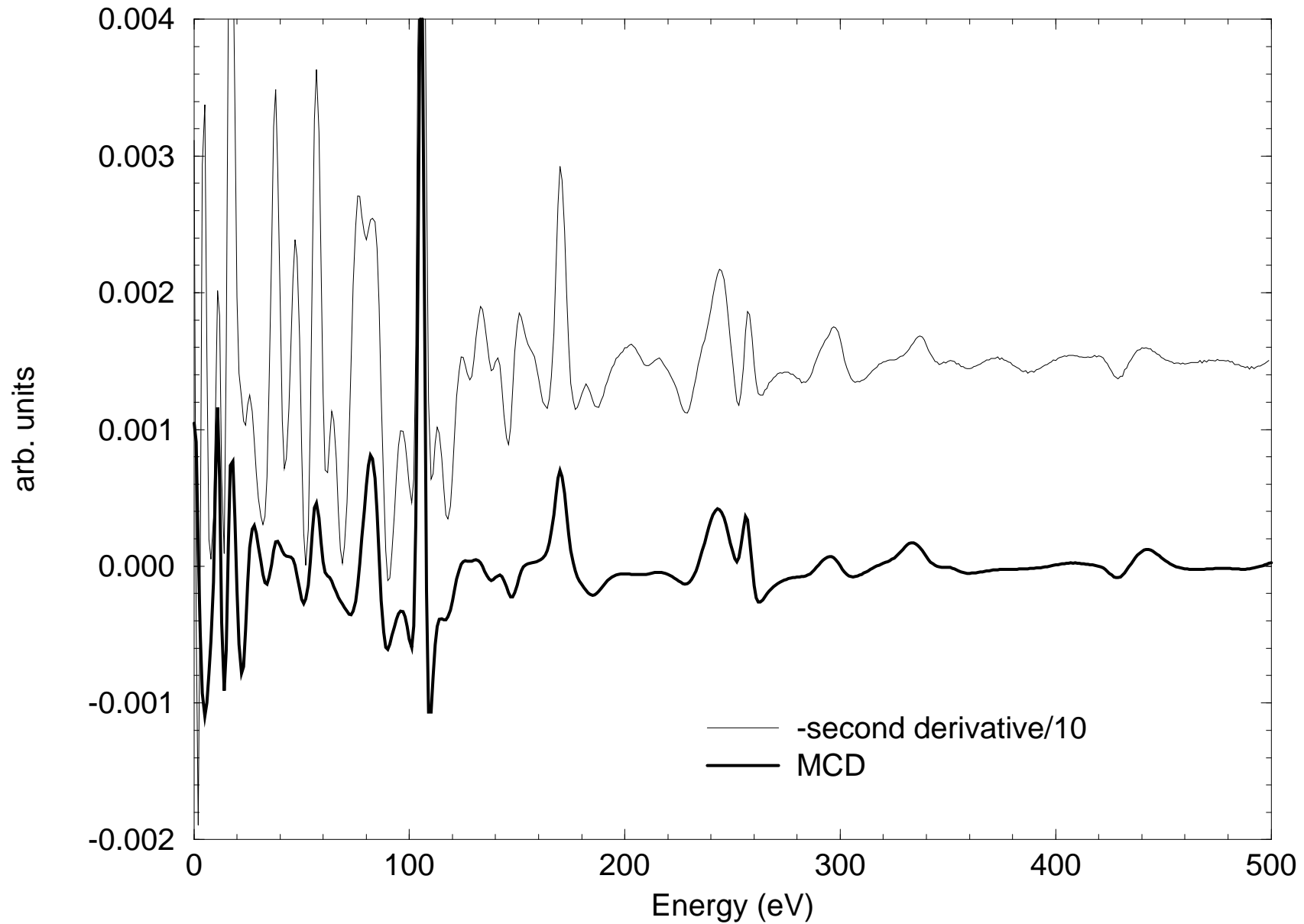
p-SDOS vs MCD

Fe bcc 51 atoms $l=8$



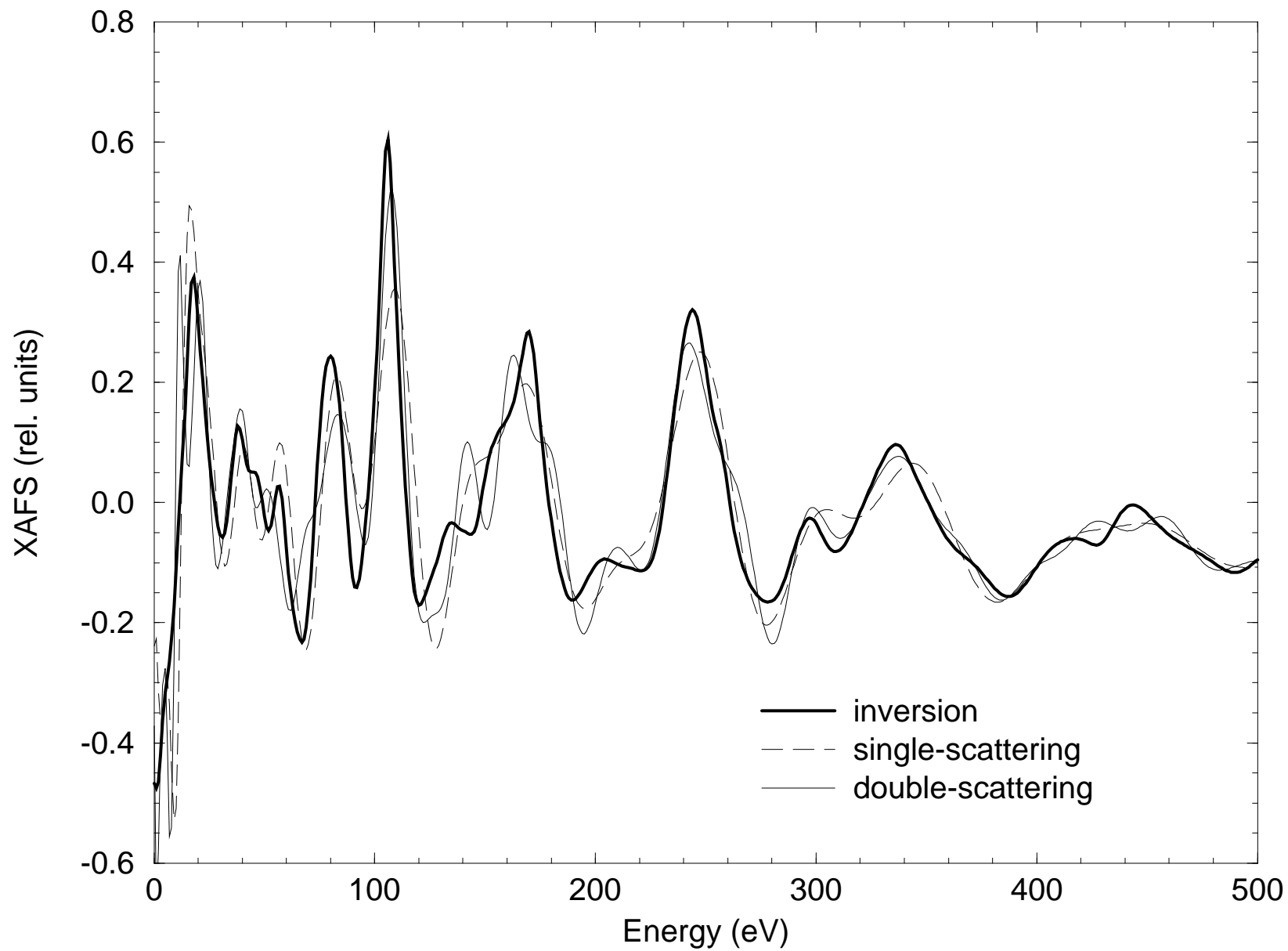
Rigid band model

bcc-Fe 51 atoms $l=8$



Multiple-scattering : XAFS

bcc-Fe 51 atoms l=8



Multiple-scattering : MCD

bcc-Fe 51 atoms $l=8$

